Check for updates

Original Article

Institution of MECHANICAL ENGINEERS

Journal of MULTI-BODY DYNAMICS

Proc IMechE Part K:
J Multi-body Dynamics
2016, Vol. 230(4) 469–488
© IMechE 2016
Reprints and permissions:
sagepub.co.uk/journalsPermissions.nav
DOI: 10.1177/1464419315627113
pik.sagepub.com
SAGE

A comparison on optimal torque vectoring strategies in overall performance enhancement of a passenger car

Seyed Mohammad Mehdi Jaafari and Kourosh Heidari Shirazi

Abstract

In this paper, a comparison is made on different torque vectoring strategies to find the best strategy in terms of improving handling, fuel consumption, stability and ride comfort performances. The torque vectoring differential strategies include superposition clutch, stationary clutch, four-wheel drive and electronic stability control. The torque vectoring differentials are implemented on an eight-DOF vehicle model and controlled using optimized fuzzy-based controllers. The vehicle model assisted with the Pacejka tyre model, an eight-cylinder dynamic model for engine, and a five-speed transmission system. Bee's Algorithm is employed to optimize the fuzzy controller to ensure each torque vectoring differential works in its best state. The controller actuates the electronic clutches of the torque vectoring differential to minimize the yaw rate error and limiting the side-slip angle in stability region. To estimate side-slip angle and cornering stiffness, a combined observer is designed based on full order observer and recursive least square method. To validate the results, a realistic car model is built in Carsim package. The final model is tested using a co-simulation between Matlab and Carsim. According to the results, the torque vectoring differential shows better handling compared to electronic stability control, while electronic stability control is more effective in improving the stability in critical situation. Among the torque vectoring differential strategies, stationary clutch in handling and four-wheel drive in fuel consumption as well as ride comfort have better operation and more enhancements.

Keywords

Vehicle handling, vehicle stability, yaw moment control, torque-vectoring differential, ride comfort

Date received: 21 October 2015; accepted: 21 December 2015

Introduction

In recent years, torque control systems have been increasingly used to improve vehicle performance, safety and pollutant emission. These systems generate additional yaw moment to correct the vehicle lateral behaviour by asymmetric distribution of traction-braking forces.[1–4] Nowadays, due to concerns over safety, the electronic stability control system (ESC) is extensively applied as a standard option of the new brands of the car producers. Regarding to the dynamic situations, this system independently activates each brake to return the vehicle to the stability margin. Researches show that ESC plays a significant role in improving vehicle stability and reducing fatal crashes.[5] However, use of ESC often raises some problems. Besides the decrease of the longitudinal performances, ESC increases fuel consumption.[2,3,6] Asymmetric distribution of traction force using torque vectoring differentials could be a solution. These systems are able to actively transfer appropriate controlled torque to each wheel, without braking.[2,7,8] Transferring the driving torque to inner wheels leads to more understeering, and for outer wheels it leads to oversteering. In spite of this excellent control of cornering performance, which comes from utilizing the live axles and active differentials, the total applied torque has merely a little difference with that of applied in the conventional differentials. Several strategies for torque-vectoring differential (TVD) have been proposed. All of these strategies use one or two clutches for generating asymmetric torque distribution.[8–10]

Studies on the direct yaw moment control can be traced back to the early 1990s. Shibahata et al.[1]

Faculty of Engineering, Mechanical Engineering Department, Shahid Chamran University, Ahvaz, Iran

Corresponding author:
Seyed Mohammad Mehdi Jaafari, Faculty of Engineering, Mechanical Engineering Department, Shahid Chamran University, Ahvaz, Iran.
Email: smm.jaafari@yahoo.com

showed that the direct yaw moment control with proper distribution of traction and braking forces on the right and left wheels provides a very effective means to improve handling, stability and vehicle manoeuvrability. Motoyama et al.[11] made an experimental vehicle that controlled the traction force distribution to each of the four wheels and showed that control of the traction distribution between the left and right wheels greatly influences turning characteristics even in a marginal turning condition. Ikushima and Sawase[12] proposed a system for left–right torque distribution that had the ability to correct the vehicle yaw moment, regardless of vehicle acceleration or deceleration. Sawase and Sano[8] from Mitsubishi Motors introduced active yaw control (AYC) system as the first torque vectoring differential, and investigated the influence of this system on improvement of vehicle stability and handling. Hancock et al.[13] did a comparison between AYC and ESC from energy loss point of view. The results indicated high energy loss in vehicles equipped with ESC system. Deur et al.[14] presented a unified mathematical model of active differential dynamics using the bond graph modelling technique.

The present work is an investigation on the effects of different TVD strategies of a four-wheel drive vehicle in enhancement of longitudinal and lateral performances, ride comfort and energy losses. To this end, an eight degrees of freedom model is extended for vehicle and Pacejka[15] combined slip model for tyres. To ensure the best operation of each TVD, a fuzzy controller for each system is considered and optimized with fuzzy rules and the orientation of the membership functions as optimization parameters, using Bee's Algorithm.

The paper is organized in 11 sections. In sections 2 and 3, the vehicle, tyre, engine, transmission system and the different TVD's models are introduced and discussed. In sections 4–7 the controller is designed based on the optimal fuzzy scheme. Bee's algorithm (BA) is used as for fuzzy membership function optimization in section 8. In section 10, the behaviour of each TVD strategies as well as ESC during cornering in standard manoeuvres is studied. Finally, in section 11, the concluding remarks are presented.

Non-linear vehicle model

The vehicle dynamics

In the beginning of the section, several assumptions are made.

- Considering speed range of the vehicle, the Pacejka[15] steady-state model is used for simulation of dynamic interaction of the tyre and road. However, it should be noted that for higher speeds and changing road and tyre conditions, transient tyre models[16,17] in which the vehicle yaw motion and oscillatory behaviour of the road friction force in cornering manoeuvres are taken into account, yields more accurate results.
- The wheels are assumed to be rigid. So the distance of each wheel's centre to the ground remains constant during cornering manoeuvres. However, the wheels' elasticity should be considered if investigation of ride comfort of the suspension system is the main purpose. For more detail, the readers are recommended to refer to Hegazy et al.[18]
- In the present work, the effect of power transmission system dynamic on the overall motion of the vehicle is considered. The engine is an eight cylinders spark ignition type. The clutch has stribeck friction model. Although this is not the case in this research, to study the nonlinear vibration of power transmission system it is better to employ more accurate models of clutch friction.[19] The power train followed by different types of differentials.
- Since to validate the presented models it is necessary to compare the dynamic response of the vehicle with those obtained from Carsim,[20] the steering input data for the standard manoeuvres are selected based on those of used by Carsim.

Figure 1 shows a schematic diagram of an 8 DOF vehicle model including longitudinal and lateral speed (v_x, v_y), roll and yaw rates ($\dot{\varphi}$ and r) and spin motion of each wheel ($\omega_{LF}, \omega_{RF}, \omega_{LR}, \omega_{RR}$). The equations of motion according to Figure 1 can be summarized as the equations (1) to (4)

$$F_{LLF}\cos(\delta_f) + F_{LRF}\cos(\delta_f) - F_{CLF}\sin(\delta_f) - F_{CRF}\sin(\delta_f) + F_{LLR} + F_{LRR} = m_u({}^u\vec{a}_{G_u}(i)) + m_s({}^u\vec{a}_{G_s}(i)) \quad (1)$$

$$F_{CLF}\cos(\delta_f) + F_{CRF}\cos(\delta_f) + F_{LLF}\sin(\delta_f) + F_{LRF}\sin(\delta_f) + F_{CLR} + F_{CRR} = m_u({}^u\vec{a}_{G_u}(j)) + m_s({}^u\vec{a}_{G_s}(j)) \quad (2)$$

$$(F_{LRF}\cos(\delta_f) - F_{CRF}\sin(\delta_f) + F_{LRR} + F_{CLF}\sin(\delta_f) - F_{LLF}\cos(\delta_f) - F_{LLR})\frac{t}{2} + (F_{CLF}\cos(\delta_f) + F_{CRF}\cos(\delta_f) + F_{LLF}\sin(\delta_f) + F_{LRF}\sin(\delta_f))a - (F_{CLR} + F_{CRR})b + (M_{ZLF} + M_{ZRF} + M_{ZLR} + M_{ZRR}) - (h_s m_s {}^u\vec{a}_{G_s}(i))\sin(\varphi) + x_u m_u(\dot{v}_y + \dot{\theta}v_x) = I_z^u\ddot{\theta} + {}^s\dot{\vec{H}}_{G_s}(k)\cos(\varphi) + {}^s\dot{\vec{H}}_{G_s}(j)\sin(\varphi) \quad (3)$$

$$m_s g h_s \sin(\varphi) - (d_f + d_r)\dot{\varphi} - (k_f + k_r)\varphi + h_s(\cos(\varphi)m_s{}^u\vec{a}_{G_s}(j) + \sin(\varphi)m_s{}^u\vec{a}_{G_s}(k)) = {}^s\dot{\vec{H}}_{G_s}(i) \quad (4)$$

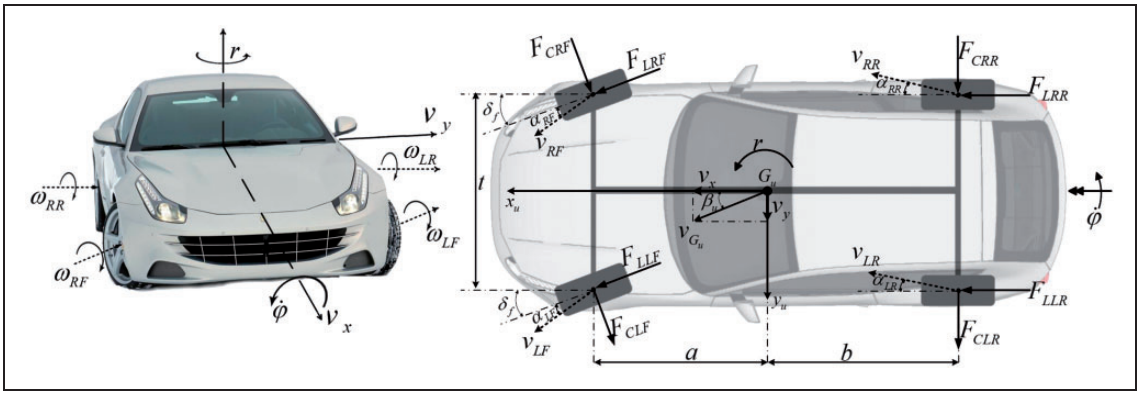

Figure 1. Eight DOF vehicle model.

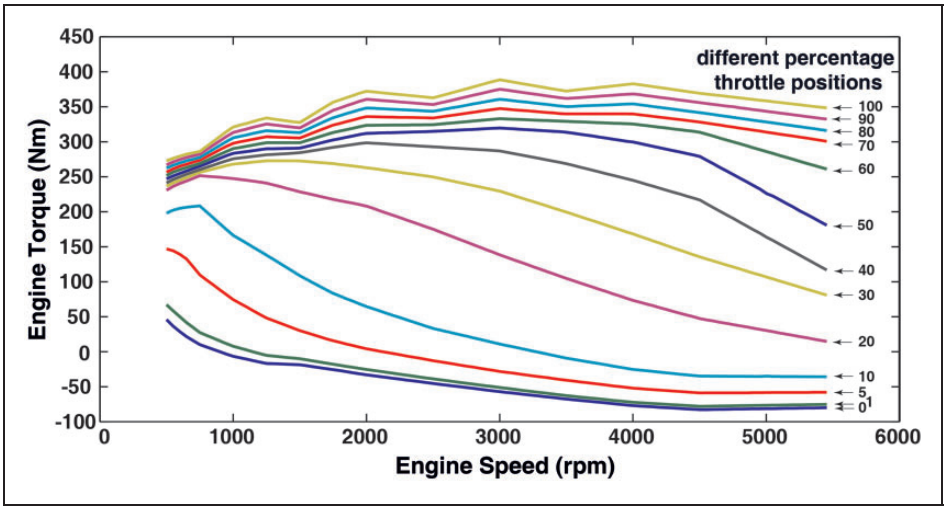

Figure 2. Engine torque map.

where ${}^{u}\vec{a}_{G_u}(i)$, ${}^{u}\vec{a}_{G_u}(j)$, ${}^{u}\vec{a}_{G_s}(i)$, ${}^{u}\vec{a}_{G_s}(j)$, ${}^{s}\dot{\vec{H}}_{G_s}(i)$, ${}^{s}\dot{\vec{H}}_{G_s}(j)$, ${}^{s}\dot{\vec{H}}_{G_s}(k)$ and related equations to the wheels are explained in Appendix 2.

The tyre and engine models

In order to simulate nonlinear behaviour of the tyres, the Pacejka[15] combined slip tyre model has been used. The general form of the formulae is as follows

$$Y(x) = D\sin(C\tan^{-1}\{Bx - E(Bx - \tan^{-1}(Bx))\}) \tag{5}$$

In equation (5), $Y(x)$ is either longitudinal force with x as longitudinal slip ratio or lateral force with x as slip angle or the self-aligning moment with x as the slip angle. The above equation parameters depend on the type of the tyre and road conditions. In this research, a 195/65 R15 tyre is used. This study ignores the transient tyre behaviour, camber angle and turn-slip in tyre model. The inputs for this model are longitudinal slip, slip angle and vertical tyre loads which are described in Appendix 2. The outputs are longitudinal tyre force, lateral tyre force and self-aligning moment which are used in equations of motion (equations (1) to (4)). The engine output torque is calculated as follows

$$T_e = f(\omega_e, \beta_{thr}). \tag{6}$$

In equation (6), T_e is the output torque, ω_e is the engine speed and β_{thr} is different percentage of throttle position. The engine used in this study is an eight cylinder with a torque map characteristic which is depicted in Figure 2.[21] A five-speed transmission system is considered and its gear ratio is given in Table 1.

Torque vectoring systems

In this research, three types of torque vectoring differential mechanisms are considered and compared with ESC system. All these systems have one or two clutches by which the asymmetric torque distribution between the axles is made possible.[8–10] When two clutch plates with different rotational speeds are compressed against each other, the torque is transferred

from the faster disc to the slower one. The transferred torque is proportional to compression force and this is the basic principle behind the TVDs.

The clutch model

Frictional torque transmitted by the clutch is a function of the normal compression force on each disc (F_c), number of active friction surfaces (n_c), the clutch friction surface radius (r_c) and friction coefficient (μ_F) which generally depends on the clutch relative speed and calculated from equation (7)[22]

$$T_F = F_c r_c n_c \mu_F = T_{req} \mu_F \tag{7}$$

where T_{req} is hydraulic torque and (μ_F) can be described by the generalized Stribeck friction model[3]. The Stribeck friction model and the parameters used are given in Appendix 2. A delay of 0.2 s is used as the differential actuator time lag. Also, the Karnopp clutch friction model is used for zero-speed region (locked mode).[23]

The SPC-TVD mechanism

In addition to ordinary differential, this system consists of two clutches and a speed increasing–decreasing gear for transferring the torque to the slower or faster wheel. It is assumed that this system is used in the rear axle of a 4WD vehicle (Figure 3) and an open differential is used in the front axle.

Table 1. Transmission ratios.

Gear	1	2	3	4	5
Gear ratio	3.42	2.14	1.45	1.03	0.81

The torque can be transferred to the faster wheel, provided that the faster wheel speed does not exceed the slower wheel speed by more than 28% (equations (8) and (9)). The relative speed between the left clutch plates and the relative speed between the right clutch plates are obtained from the equations (8) and (9), respectively. The torque transmitted to the left and right wheels is taken into account from the equations (10) and (11), respectively.

$$\omega_{f1} = \left(1 - \frac{h_1}{2}\right)\omega_2 - \frac{h_1}{2}\omega_1 \tag{8}$$

$$\omega_{f2} = \frac{h_2}{2}\omega_1 - \left(1 - \frac{h_2}{2}\right)\omega_2 \tag{9}$$

$$T_{t1} = \frac{1}{2} i T_{er} + \frac{1}{2} h_1 T_{f1} - \frac{1}{2} h_2 T_{f2} - \dot{\omega}_1 \left(\frac{1}{4} i^2 I_i^* + I_1\right) - \dot{\omega}_2 \left(\frac{1}{4} i^2 I_i^*\right) \tag{10}$$

$$T_{t2} = \frac{1}{2} i T_{er} + \left(\frac{1}{2} h_1 - 1\right) T_{f1} - \left(\frac{1}{2} h_2 - 1\right) T_{f2} - \dot{\omega}_2 \left(\frac{1}{4} i^2 I_i^* + I_2\right) - \dot{\omega}_1 \left(\frac{1}{4} i^2 I_i^*\right)$$
$$I_i^* = I_i + i^{-2}(I_c + I_{gc}^*), I_{gc}^* = I_{gc} + (h_2)^2 I_{C2} + (h_1)^2 I_{C1} - \left(\frac{Z_1}{Z_2}\right)^2 I_{dg}, \quad h_1 = \frac{Z_1 Z_6}{Z_4 Z_3}, \quad h_2 = \frac{Z_1 Z_5}{Z_4 Z_2} \tag{11}$$

The STC-TVD mechanism

This system has two stationary clutches and two series of planetary gears which are on the both output shafts

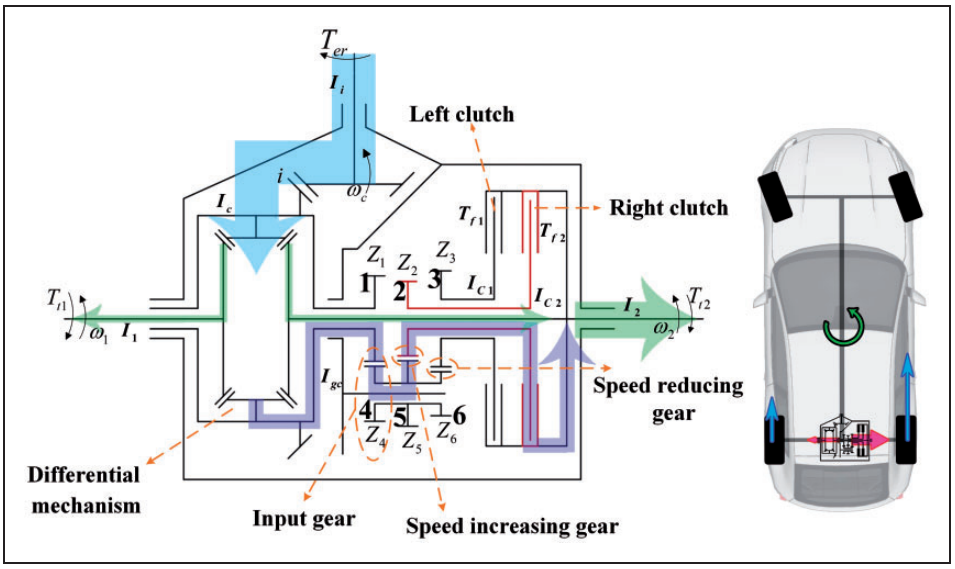

Figure 3. Kinematic schemes of SPC-TVD.

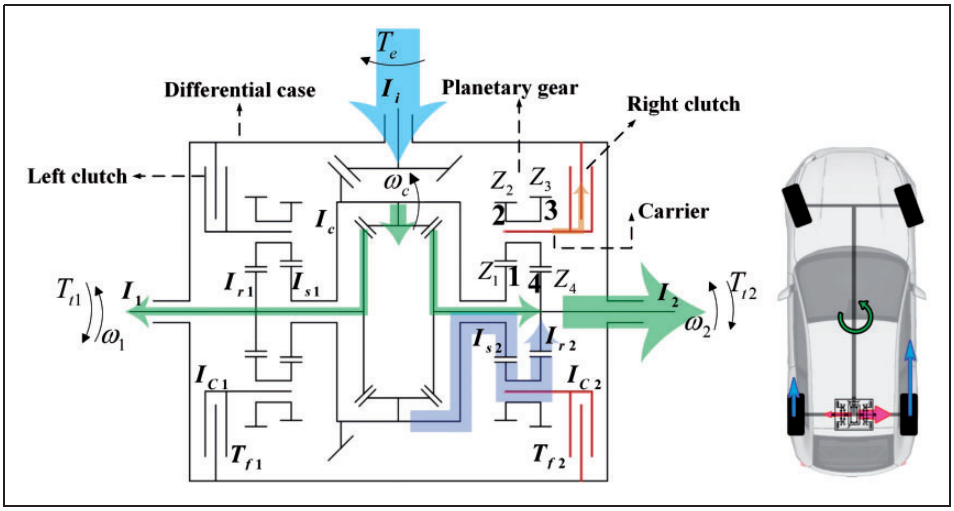

Figure 4. Kinematic schemes of STC-TVD.

of the ordinary differential (Figure 4). This differential acts like a normal differential while clutches being inactive. When the left clutch is activated, more torque is transferred to the left wheel and when the right clutch is activated, more torque is transferred to the right wheel. The demanded torque transfer to the faster wheel can be achieved if the wheel speed difference does not exceed by more than the 28% of slower wheel speed (equations (12) and (13)).

It is assumed that this system is used in the rear axle of a 4WD vehicle and in front axle an open differential is used. The relative speed between the left clutch plates and the relative speed between the right clutch plates are calculated from the equations (12) and (13), respectively. The torque transmitted to the left and right wheels is derived from the equations (14) and (15), respectively.

$$\omega_{f1} = H_{11}\omega_2 - H_{12}\omega_1 \tag{12}$$

$$\omega_{f2} = H_{21}\omega_1 - H_{22}\omega_2 \tag{13}$$

$$\begin{aligned} T_{t1} = {} & \frac{1}{2} i T_{er} + H_{12} T_{f1} - H_{21} T_{f2} \\ & - \dot{\omega}_1 \left(I_1^* + \frac{1}{4} i^2 I_i^* + H_{12}^2 I_{C1} + H_{21}^2 I_{C2} \right) \\ & - \dot{\omega}_2 \left(\frac{1}{4} i^2 I_i^* - H_{11} H_{12} I_{C1} - H_{21} H_{22} I_{C2} \right) \end{aligned} \tag{14}$$

$$\begin{aligned} T_{t2} = {} & \frac{1}{2} i T_{er} + H_{22} T_{f2} - H_{11} T_{f1} \\ & - \dot{\omega}_1 \left(\frac{1}{4} i^2 I_i^* - H_{11} H_{12} I_{C1} - H_{21} H_{22} I_{C2} \right) \\ & - \dot{\omega}_2 \left(I_2^* + \frac{1}{4} i^2 I_i^* + H_{11}^2 I_{C1} + H_{22}^2 I_{C2} \right) \end{aligned}$$

$$h_1 = h_2 = \frac{Z_1 Z_3}{Z_2 Z_4}, \quad H_{11} = \frac{h_1}{2(h_1 - 1)}, \quad H_{12} = \frac{2 - h_1}{2(h_1 - 1)},$$

$$\begin{aligned} & H_{21} = \frac{h_2}{2(h_2 - 1)}, \quad H_{22} = \frac{2 - h_2}{2(h_2 - 1)}, \\ & I_i^* = I_i + i^{-2}(I_c + I_{s1} + I_{s2}), \quad I_{s2} = I_{s1}, \\ & I_1^* = I_1 + I_{r1}, I_2^* = I_2 + I_{r2}, \quad I_{r2} = I_{r1}. \end{aligned} \tag{15}$$

The 4WD-TVD mechanism

This differential is particularly designed for using in 4WD vehicles, which possesses two stationary clutches and two sets of planetary gears. This system is not built around the traditional open differential and when the clutches are disengaged, the output torque is equal to zero. Through the simultaneous control of both clutches, torque distribution between the front and rear axle is adjusted and by the independent control of each clutch, the torque between the left and right wheels is regulated (Figure 5).

The relative speed between the left clutch discs and the relative speed between the right clutch discs are calculated from the equations (16) and (17), respectively. The torque transmitted to the four wheels is taken into account from the equations (18) to (21).

$$\omega_{f1} = G_1\omega_3 + G_1\omega_4 - \omega_1(1 + h_1) \tag{16}$$

$$\begin{aligned} & \omega_{f2} = G_2\omega_3 + G_2\omega_4 - \omega_2(1 + h_2) \\ & h_1 = \frac{Z_r}{Z_s}, \quad G_1 = h_1 \frac{g_i i_f}{2 i_r}, \quad h_2 = \frac{Z_r}{Z_s}, \quad G_2 = h_2 \frac{g_i i_f}{2 i_r}, \\ & i_r = i_f \frac{h_1}{h_1 + 1} \end{aligned} \tag{17}$$

$$\begin{aligned} T_{t1} = {} & T_{f1}(1 + h_1) + \dot{\omega}_3 G_1 I_{s1}(1 + h_1) + \dot{\omega}_4 G_1 I_{s1}(1 + h_1) \\ & - \dot{\omega}_1 (I_1^* + I_{s1}(1 + h_1)^2) \end{aligned} \tag{18}$$

$$\begin{aligned} T_{t2} = {} & T_{f2}(1 + h_2) + \dot{\omega}_3 G_2 I_{s2}(1 + h_2) + \dot{\omega}_4 G_2 I_{s2}(1 + h_2) \\ & - \dot{\omega}_2 (I_2^* + I_{s2}(1 + h_2)^2) \end{aligned} \tag{19}$$

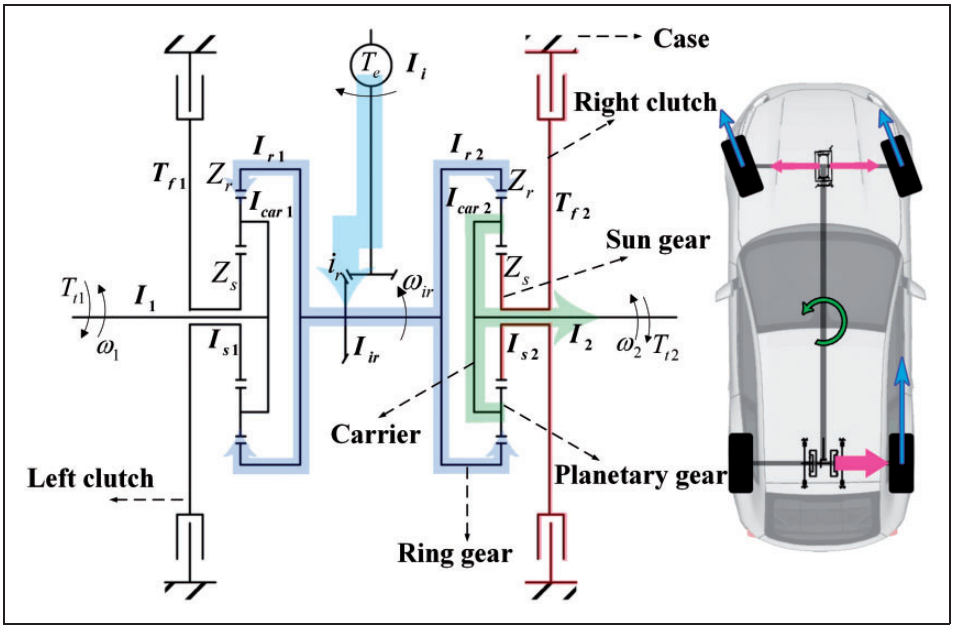

Figure 5. Kinematic schemes of 4WD TVD.

$$T_{t3} = \frac{1}{2} i_f T_e - T_{f1} G_1 - T_{f2} G_2 + \dot{\omega}_1 G_1 I_{s1}(1 + h_1) + \dot{\omega}_2 G_2 I_{s2}(1 + h_2) - \dot{\omega}_3 (J + I_3) - \dot{\omega}_4 J \quad (20)$$

$$T_{t4} = \frac{1}{2} i_f T_e - T_{f1} G_1 - T_{f2} G_2 + \dot{\omega}_1 G_1 I_{s1}(1 + h_1) + \dot{\omega}_2 G_2 I_{s2}(1 + h_2) - \dot{\omega}_4 (J + I_4) - \dot{\omega}_3 J$$

$$I_1^* = I_1 + I_{car1},$$

$$J = I_{s1} G_1^2 + I_{s2} G_2^2 + (i_f^2/4) I_i^*$$

$$I_i^* = I_i + I_{cf}/i_f^2 + (g_i/i_r)^2 (I_{ir} + I_{r1} + I_{r2}),$$

$$I_2^* = I_2 + I_{car2}$$

$$h_1 = \frac{Z_r}{Z_s}, \quad G_1 = h_1 \frac{g_i i_f}{2 i_r}, \quad h_2 = \frac{Z_r}{Z_s},$$

$$G_2 = h_2 \frac{g_i i_f}{2 i_r}, \quad i_r = i_f \frac{h_1}{h_1 + 1} \quad (21)$$

The parameter values used in the vehicle model and active differentials are given in Appendix 3.

The ESC system

Creating differential braking by increasing the brake pressure at the left wheels compared to the right wheels generates a counter-clockwise yaw moment and vice versa. In the understeering situation, braking force is applied on the inside rear wheel and in the oversteering situation the braking force is applied on the outside front wheel.[24] In this research, the vehicle equipped with ESC has open differential in both front and rear axles.

The controller

The purpose of controller here is to track the desired yaw motion and limit the side-slip angle within the stability region. At high slip angles, the tyres lose their linear behaviour and approach the limit of adhesion. It is pointed out that on dry asphalt roads, the limitation reached at a side-slip angle of approximately ±12°, while on packed snow roads, this value is about ±2°.[25] The control algorithm is fuzzy due to fast response and simplicity in implementation. The following empirical relation is suggested as the critical side-slip angle of the vehicle for stability.[26]

$$\beta_{critical} = \tan^{-1}(0.02\,\mu g) \quad (22)$$

where μ is the road friction coefficient. This relation yields an upper bound of 10 degrees at a friction coefficient of $\mu = 0.9$ and an upper bound of four degrees at a friction coefficient of $\mu = 0.35$. In this research, low, medium and high side-slip angles are defined as follows

$$\text{Low side-slip angle}: |\beta| \leqslant \frac{1}{3}\beta_{critical} \quad (23)$$

$$\text{Medium side-slip angle}: \frac{1}{3}\beta_{critical} < |\beta| \leqslant \frac{2}{3}\beta_{critical} \quad (24)$$

$$\text{High side-slip angle}: \frac{2}{3}\beta_{critical} < |\beta|. \quad (25)$$

A desired yaw rate can be defined based on the driver's steering input, bicycle model and vehicle speed from equation (26)[26,27]

$$r_d = \frac{v_x \delta}{(b + a) + K_u v_x^2}, \quad K_u = \frac{M}{b + a}\left(\frac{b}{C_f} - \frac{a}{C_r}\right) \quad (26)$$

where M is the vehicle mass and (v_x) is longitudinal speed taken from vehicle model. Considering the tyre–road friction coefficient, the desired yaw rate r_d must comply with the following conditions[25,26]

$$|r_d| < \left|\frac{\mu g}{v_x}\right| \tag{27}$$

where C_f and C_r are the front and rear cornering stiffness, respectively. The fuzzy inputs are side-slip angle (β), yaw rate error ($e = r - r_d$) and its derivative ($\dot{e} = \dot{r} - \dot{r}_d$) and the output is clutch torque, T_{req} in equation (7). Obviously, by choosing n_c and r_c by the designer, the force needed to push the clutch is derived from $T_{req}/n_c r_c$ (equation (7)). The vehicle yaw rate (r) is taken from vehicle model and the side-slip is estimated from the measured vehicle states. The control system decides to switch the appropriate clutching in the torque vectoring differentials or appropriate tyres for braking in ESC. Moreover, the allowable wheel speed difference for torque distribution is controlled in this layer. The schematic diagram of the control system is depicted in Figure 6.

It should be noted that to minimize the total clutch loss for the given torque transfer TVD's, only one clutch should be engaged in each time. The detail of design and optimization of fuzzy control can be seen in Appendix 4.

Fuel consumption and energy considerations

The energy dissipated during each of the manoeuvres is taken into account from equation (28)[3]

$$E_d = \sum_{i=RF,LF,RR,LR} \left(\int F_{Li}(r_i\omega_i - U_{wi})\mathrm{d}t + \int F_{Ci}V_{wi}\mathrm{d}t + \int T_{Bi}\omega_i \mathrm{d}t \right) + \sum_{i=1}^{2} \int T_{fi}\omega_{fi}\mathrm{d}t \tag{28}$$

where E_d is dissipated energy. The integrand terms are energy losses due to tyre longitudinal slip, tyre lateral slip, brakes and differential clutches. Also, the energy losses can be obtained by subtracting the total kinetic energy from the power train energy as given in the equation (29). Both equations (28) and (29) give the same result.

$$E_d = \int T_e\omega_e \mathrm{d}t - \left[\frac{1}{2}\left[M(v_x^2 + v_y^2) + (I_z^s + I_z^u)\dot{\theta}^2 + I_x^s\dot{\varphi}^2 + \sum_{i=1}^{4} I_w\omega_i^2 - M(v_{x0}^2 + v_{y0}^2)\right] + K_{Trans}\right] \tag{29}$$

Model validation

In order to validate the vehicle model, the dynamic responses including vehicle path, yaw rate, rolling angle, and side slip angle under the fishhook manoeuvre are obtained and compared with those of Carsim built model. As it can see in Figure 7, both the 8-DOF model and Carsim model have very similar dynamic behaviour. Therefore, the model is prepared to be used in the optimum fuzzy control design process. The main reason for using 8-DOF model rather than Carsim model is its efficient execution time. This property makes it suitable for performing a design process based on optimization.

Parameter estimation

In order to estimate the side-slip angle and the cornering stiffness in equation (26), a combined observer

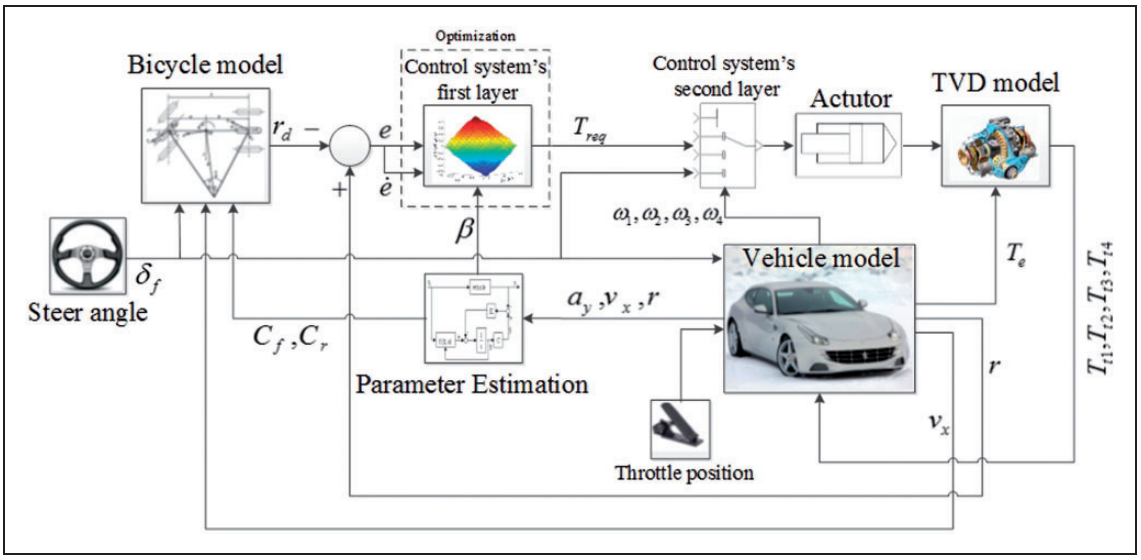

Figure 6. Schematic diagram of control system.

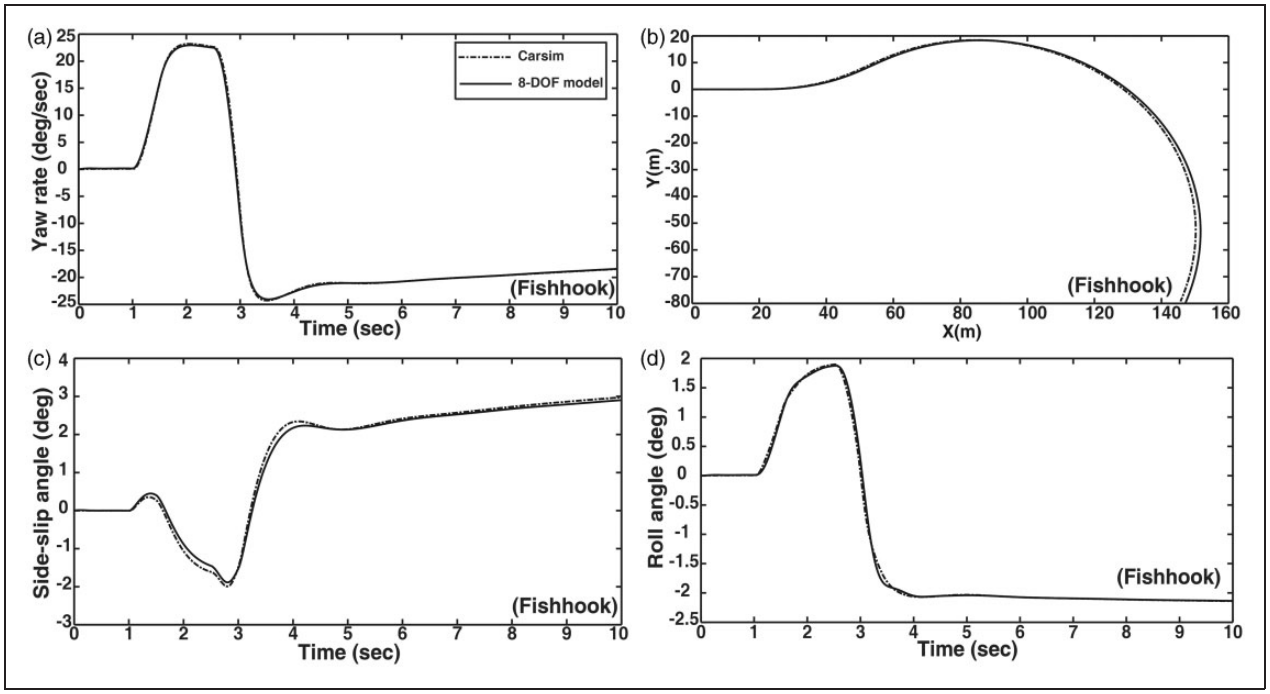

Figure 7. Comparison of the vehicle responses for the 8-DOF model and the Carsim model.

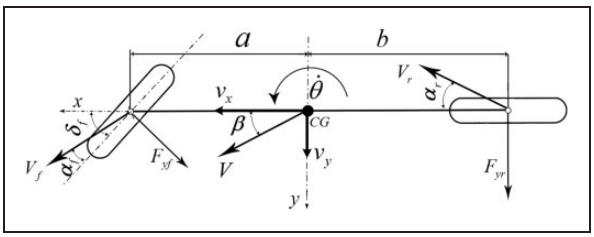

Figure 8. Bicycle model.

based on full-order observer and recursive least square method is used.

Side-slip angle estimation

The 2-DOF vehicle model (bicycle model) with constant speed is adopted to estimate the side-slip angle. The bicycle model does not consider the tyre tangential force and ignores the load transfer of the vehicle and the air resistance. Figure 8 shows the bicycle model.

Assuming the vehicle side-slip angle (β) and the steer angle of the front wheel (δ_f) are small, the vehicle formulas are obtained as follows[26]

$$ma_y = 2C_f\left(\delta_f - \beta - \frac{r}{v_x}a\right) + 2C_r\left(\frac{r}{v_x}b - \beta\right) \tag{30}$$

$$I_z\dot{r} = 2aC_f\left(\delta_f - \beta - \frac{r}{v_x}a\right) - 2bC_r\left(\frac{r}{v_x}b - \beta\right). \tag{31}$$

Side-slip angle β and yaw rate r are used as state variables, and lateral acceleration a_y and yaw rate are used as system measurement variables. Equations (30) and (31) can be expressed as state–space form

$$\dot{x} = Ax + Bu \tag{32}$$

$$y = Cx + Du \tag{33}$$

where

$$x = \begin{bmatrix} \beta \\ r \end{bmatrix}, \quad u = \begin{bmatrix} \delta_f \\ 0 \end{bmatrix}, \quad y = \begin{bmatrix} r \\ a_y \end{bmatrix} \tag{34}$$

$$A = \begin{bmatrix} -\dfrac{2(C_f + C_r)}{mv_x} & -\dfrac{2aC_f - 2bC_r}{mv_x^2} - 1 \\ -\dfrac{2(aC_f - bC_r)}{I_z} & -\dfrac{2(a^2C_f + b^2C_r)}{I_z v_x} \end{bmatrix},$$
$$B = \begin{bmatrix} \dfrac{2C_f}{mv_x} & 0 \\ \dfrac{2aC_f}{I_z} & \dfrac{1}{I_z} \end{bmatrix} \tag{35}$$

$$C = \begin{bmatrix} 0 & 1 \\ -\dfrac{2(C_f + C_r)}{m} & -\dfrac{2(aC_f - bC_r)}{mv_x} \end{bmatrix},$$
$$D = \begin{bmatrix} 0 & 0 \\ \dfrac{2C_f}{m} & 0 \end{bmatrix} \tag{36}$$

Then, the state–space observer dynamic equation can be obtained using the state observer theory[28]

$$\dot{\hat{x}} = A\hat{x} + Bu - K(\hat{y} - y) \tag{37}$$

$$\hat{y} = C\hat{x} + Du \tag{38}$$

where K is observer matrix gain. For high response and robustness purposes, K is selected as follows[29]

$$K = \begin{bmatrix} \frac{1}{4}\frac{(2aC_f - 2bC_r)\lambda_1\lambda_2 I_z}{C_f C_r (a+b)^2} - 1 & \frac{1}{v_x} \\ -\lambda_1 - \lambda_2 & \frac{m(a^2 C_f + b^2 C_r)}{I_z(aC_f - bC_r)} \end{bmatrix} \tag{39}$$

in which λ_1 and λ_2 are the assigned pole values of the observer. The diagram of designed observer is shown in Figure 9.

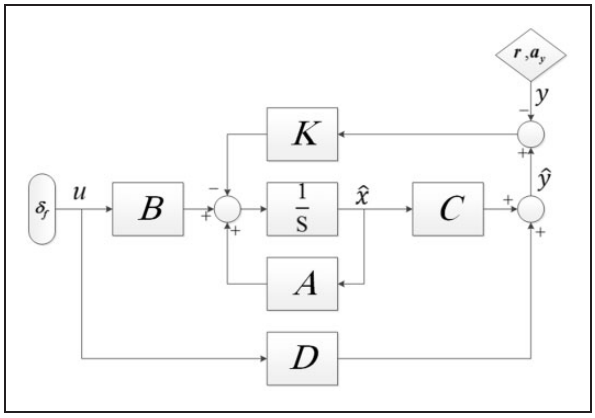

Figure 9. Structure of observer for side-slip angle.

Cornering stiffness estimation

To estimate the cornering stiffness, the recursive least square method has been used. In least square estimation, unknown parameters of a linear model are chosen in such a way that the sum of the squares of the difference between the actually observed and the computed values is minimum. Equations (40) to (44)

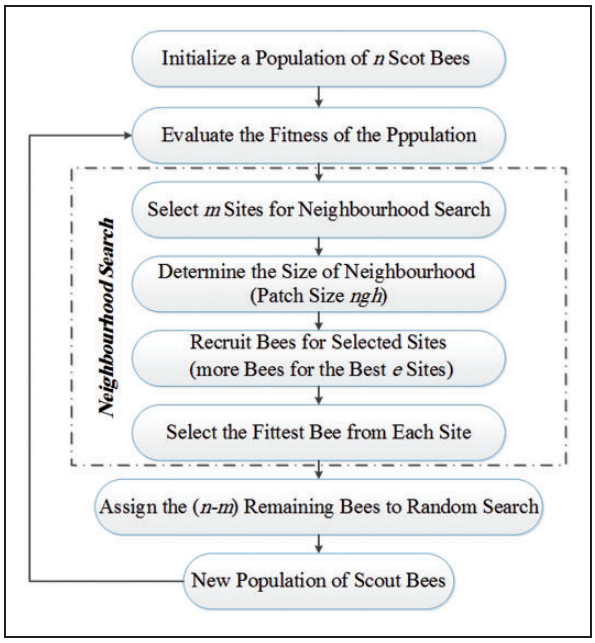

Figure 11. Flowchart of BA algorithm.

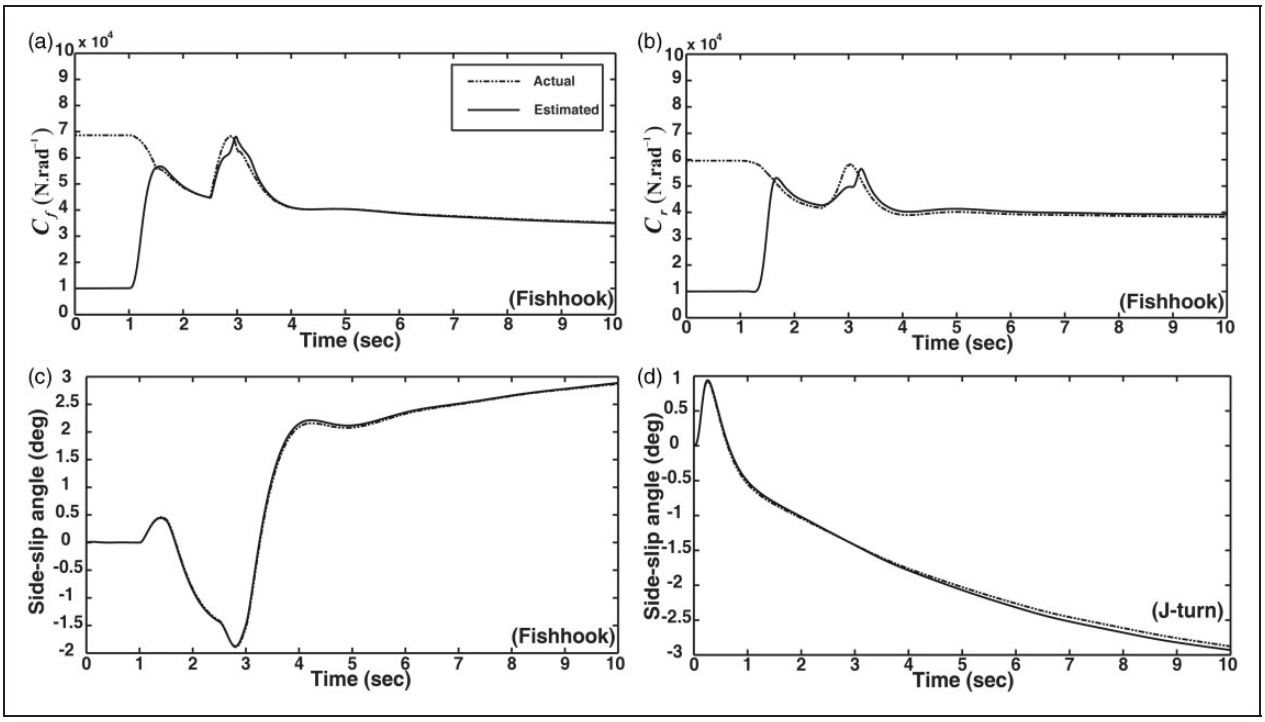

Figure 10. Actual and estimated parameters.

explain the method

$$y(t) = \varphi^T(t)\theta(t) \tag{40}$$

$$e(t) = y(t) - \varphi^T(t)\hat{\theta}(t) \tag{41}$$

$$\frac{d\hat{\theta}(t)}{dt} = P(t)\varphi(t)e(t) \tag{42}$$

$$\lambda(t) = \lambda_0\left(1 - \frac{\|P\|}{K_0}\right) \tag{43}$$

$$\frac{dP(t)}{dt} = \lambda(t)P(t) - P(t)\varphi(t)\varphi^T(t)P(t) \tag{44}$$

where $\theta(t)$ is the vector of estimated parameters, $\varphi(t)$ is the regression vector and $e(t)$ is the identification error between measured $y(t)$ and estimated value $\varphi^T(t)\hat{\theta}(t)$. The parameter λ is called the forgetting factor.[30] It operates as a weight which diminishes for the more remote data and $P(t)$ is called covariance matrix, and for the better results it is recommended to assume that $\|P\| \leqslant K_0$. Equations (30) and (31) can be rewritten in standard regression form as

$$\begin{bmatrix} a_y \\ \dot{r} \end{bmatrix} = \begin{bmatrix} \dfrac{2\left(\delta_f - \beta - \dfrac{r}{v_x}a\right)}{m} & \dfrac{2\left(\dfrac{r}{v_x}b - \beta\right)}{m} \\ \dfrac{2a\left(\delta_f - \beta - \dfrac{r}{v_x}a\right)}{I_z} & -\dfrac{2b\left(\dfrac{r}{v_x}b - \beta\right)}{I_z} \end{bmatrix} \begin{bmatrix} C_f \\ C_r \end{bmatrix}. \tag{45}$$

Then

$$y = \begin{bmatrix} a_y \\ \dot{r} \end{bmatrix}, \quad \varphi^T = \begin{bmatrix} \dfrac{2\left(\delta_f - \beta - \dfrac{r}{v_x}a\right)}{m} & \dfrac{2\left(\dfrac{r}{v_x}b - \beta\right)}{m} \\ \dfrac{2a\left(\delta_f - \beta - \dfrac{r}{v_x}a\right)}{I_z} & -\dfrac{2b\left(\dfrac{r}{v_x}b - \beta\right)}{I_z} \end{bmatrix},$$
$$\theta = \begin{bmatrix} C_f \\ C_r \end{bmatrix}. \tag{46}$$

Therefore, cornering stiffness will be determined by means of equations (40) to (46). Figure 10 shows the estimated and actual cornering stiffness and side-slip angle. It is seen from Figure 10 that the estimates of the states match well with the simulation results.

Optimization

In order to improve the controller performances, the designed controller is optimized for each TVD strategy using Bees algorithm optimization method (BA). The BA method is an optimization algorithm which is inspired from a searching behaviour of the bees.[31] The flowchart of BA algorithm is depicted in Figure 11. In this method, a population of optimization parameters (fuzzy rules and the orientation of the membership functions) with n individuals each called a bee is generated. The cost function for each bee is evaluated to show which one finds a better place for flowers. Comparing fitness function of the bees, m best places are selected and a ngh neighbourhood for each m places is defined. Then a number of bees for best e places are recruited. After that, m bees related to the best m places are selected. For n–m remaining places, again some neighbourhood is randomly defined and new population is generated.

Since the main purpose of controller is to improve the vehicle handling and vehicle stability, the objective function is obtained from the equation (47)

$$\begin{aligned} &Minimize\ F(u) \\ &where\ \ F(u) = v_1 \int |r - r_d| \mathrm{dt} \\ &\quad + \frac{1}{2}v_2 \int (|\beta| - \frac{1}{2}\beta_{critical}) + \left|(|\beta| - \frac{1}{2}\beta_{critical})\right| \mathrm{dt}, \end{aligned} \tag{47}$$

in which v_1 and v_2 are weight factors for normalization of cost function parameters. The first term of cost function is defined for minimizing the integral of yaw rate error ($e = r - r_d$) and the second term is defined to limit the side-slip angle lower than $1/2\beta_{critical}$ as much as possible. There are two layers of optimization. In the first layer, fuzzy rules are optimized. In the second layer, the skewness of the membership functions is taken to obtain best value of the cost function during a standard manoeuvre.

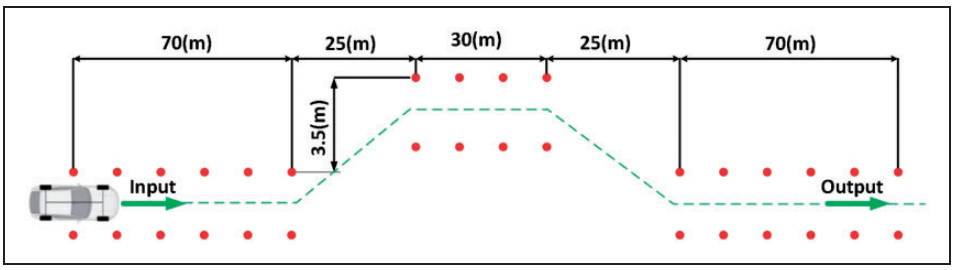

Figure 12. Desired path in DLC manoeuvre.

Manoeuvres

In order to evaluate the influence of each TVD, the vehicle undergoes standard testing including the fishhook, J turn and double lane change (DLC). The desired path in DLC manoeuvre is shown in Figure 12. Steering angle histogram for the front wheels in J turn and fishhook manoeuvre is shown in Figure 13.

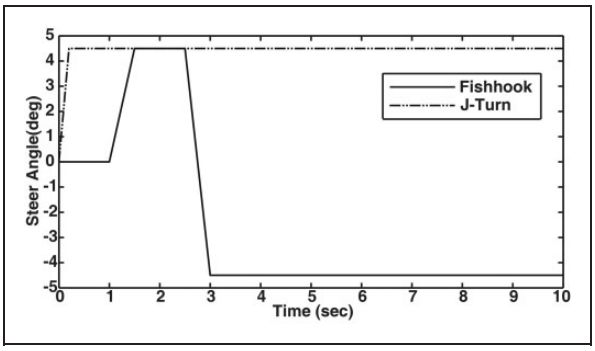

Figure 13. Steering command in front wheels in J and fishhook manoeuvre.

Discussion

Handling, stability, ride comfort and fuel consumption are four criteria for comparing the performance of the TVDs. Yaw rate error, side-slip angle and vehicle speed–acceleration are quantitative measures for handling, stability and ride comfort, respectively, and for fuel consumption (or energy losses) equation (28) is used as well. The integral of yaw rate error and the side-slip angle for different TVDs' strategies and different initial speeds are shown in Figures 14 and 15. It is seen that besides limiting the side-slip angle inside the allowable range, four TVD strategies improve the yaw rate.

Handling

Figures 14 and 15 depict that TVDs are as effective as ESC in handling improvement. In fact the TVD strategies produce the necessary yaw moment by using two wheels instead of one. However, 4WD-TVD shows weaker performance than the other, because when 4WD-TVD is activated, the torque in the

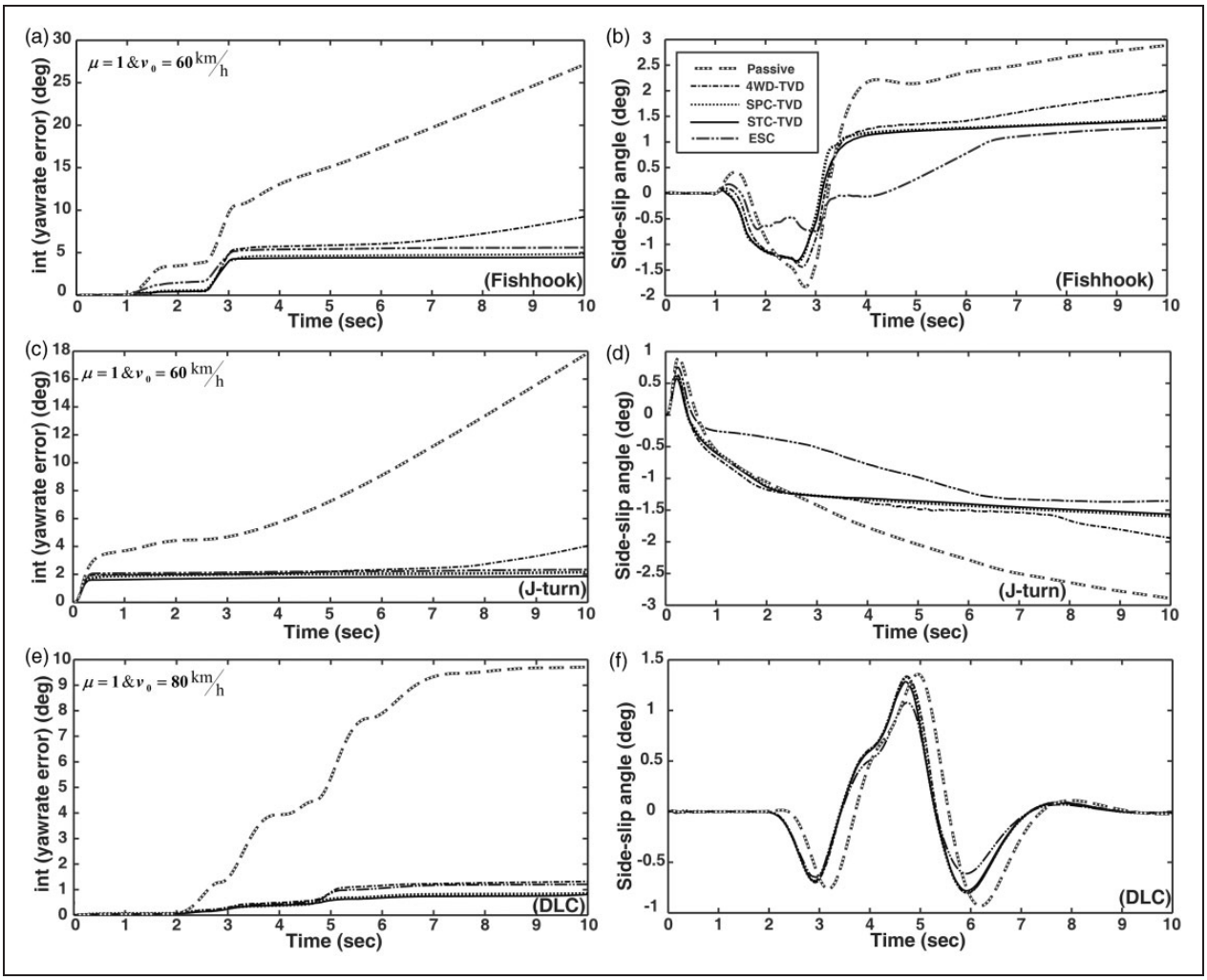

Figure 14. $\int_0^{10} |r - r_d| dt$ and side-slip angle for vehicle equipped with the torque distribution systems under medium initial speed.

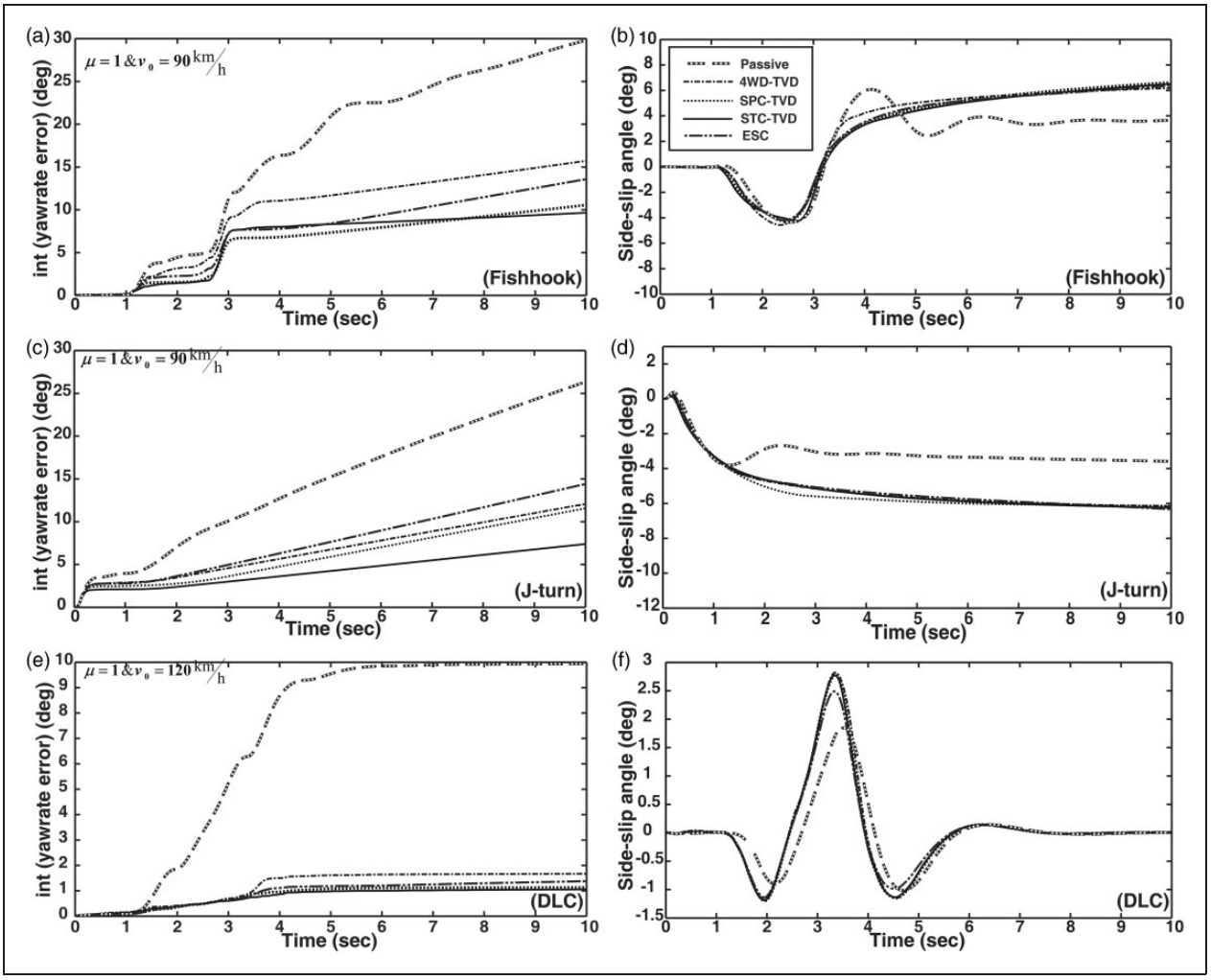

Figure 15. $\int_0^{10} |r - r_d| dt$ and side-slip angle for vehicle equipped with the torque distribution systems under high initial speed.

front axle is reduced and on the contrary it increased in the rear axle. Therefore, the handling tends to be more oversteer. Among the different TVD strategies, stationary clutch torque vectoring differential (STC-TVD) and after that superposition clutch torque vectoring differential (SPC-TVD) show the best handling performance.

Ride comfort

A weak point of ESC is speed and longitudinal acceleration reduction due to braking and as a result reduction of ride comfort as well as more fuel consumption. As a quantitative measure for ride comfort performance, both the longitudinal speed and acceleration reduction are taken into account. Figure 16 shows the longitudinal acceleration in the different TVD strategies. Obviously in all three manoeuvres, ESC dramatically reduces the ride comfort while in TVDs, the speed and acceleration reduction is negligible.

Figure 17 shows the percentage of average vehicle speed reduction compared to a conventional vehicle in investigated manoeuvres. According to this figure, the ESC has a significant reduction in average speed, while torque vectoring differential has a negligible variation on the vehicle speed. According to Figures 16 and 17, it can be said that ESC has weakest ride comfort performance while among the TVD strategies, 4WD-TVD and STC-TVD have the highest and lowest benefits, respectively. In TVDs, the total wheel torque decreased when one of the left or right clutches is activated, and thus the vehicle tends to slightly decelerate during the torque distribution process, but this reduction is much lower than ESC.

Fuel consumption (energy loss)

One of the important sources of fuel consumption is energy loss during successively braking and accelerating. From the fuel consumption point, each TVD strategy as well as ESC should be analysed and evaluated. Figure 18 depicts the energy loss during the standard manoeuvres. It is clear that the energy loss for the ESC is much larger than that of lost by all

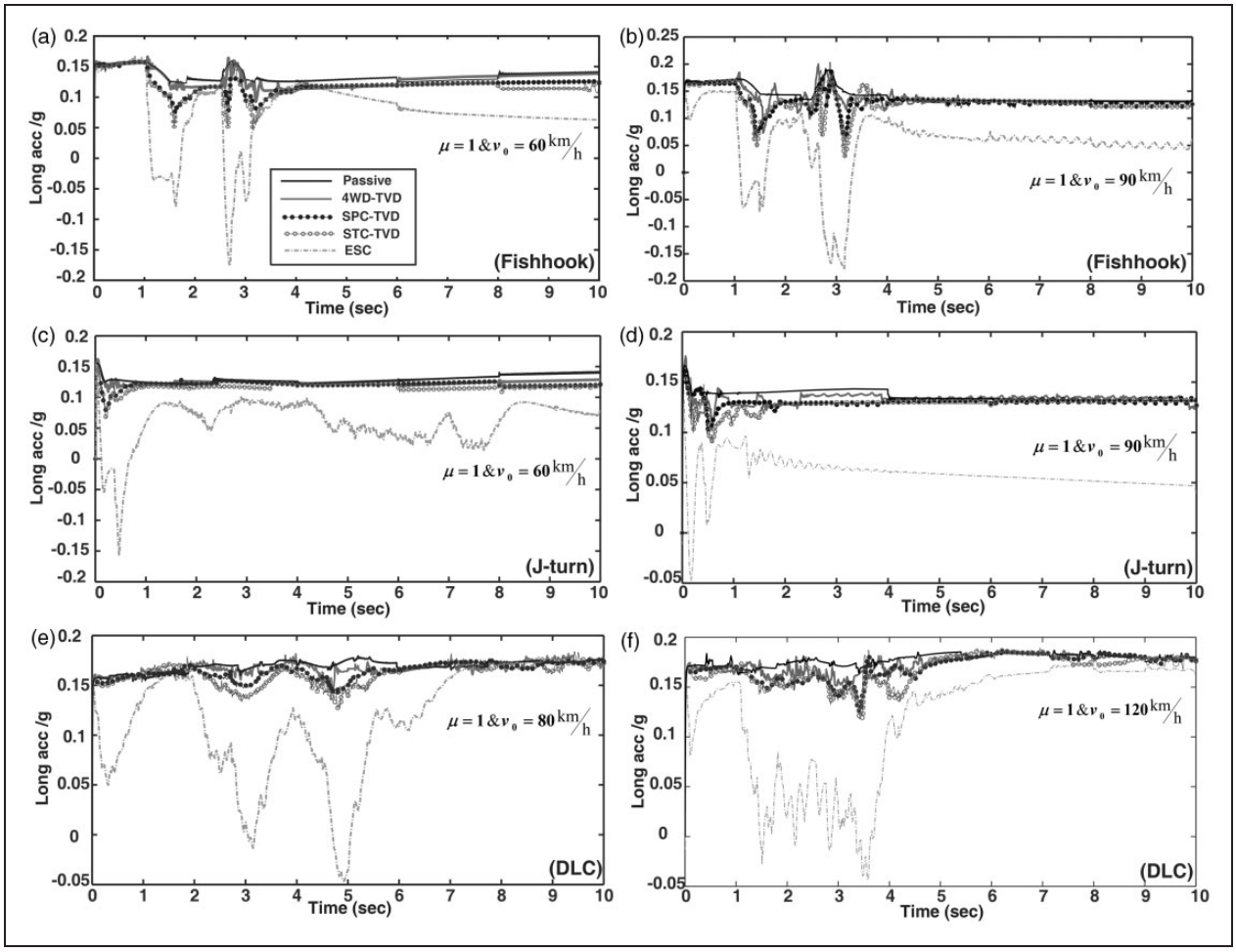

Figure 16. Longitudinal acceleration in DLC manoeuvre.

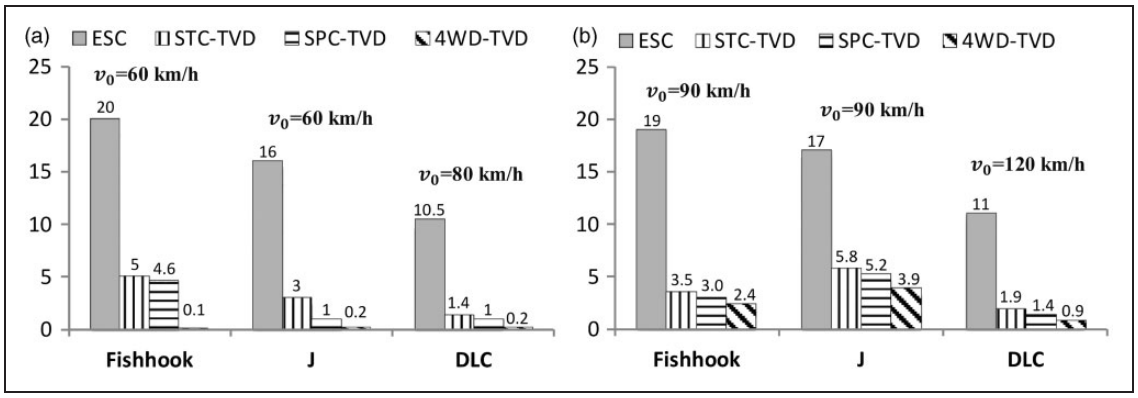

Figure 17. Percentage of average vehicle speed reduction.

kinds of TVD strategies. Among TVD strategies, STC-TVD and SPC-TVD have more energy loss in comparison with 4WD-TVD; however, this is much less than the energy loss in the ESC.

Weight and price are other important concerns of vehicle industries. One of the important items that affects the price and weight of TVDs is the type of the actuator. Figure 19 shows the integral of required actuating torque for the different TVDs.

One can see that the required actuating torque to generate corrective yaw moment in SPC-TVD is much larger than that in STC-TVD and 4WD-TVD. Accordingly, unlike 4WD-TVD and STC-TVD, a SPC-TVD requires a heavier and larger

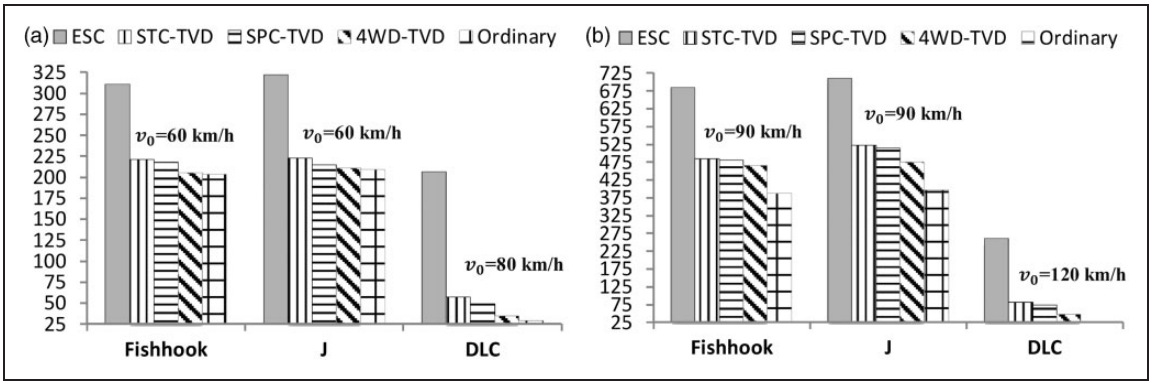

Figure 18. Energy losses (KJ).

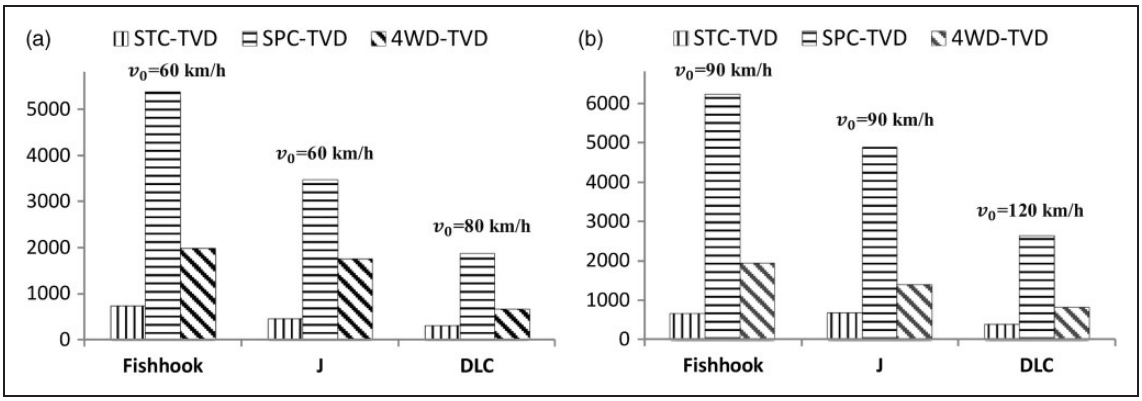

Figure 19. Actuation torque.

actuator which could be more complex and energy consuming.

Handling and stability in lower friction coefficient

Cornering stability in low friction road condition is one of the main concerns of vehicle dynamic control system designers. Figure 20 shows the integral of yaw rate error and side-slip angle of the vehicle behaviour under wet road conditions. All the four TVDs have improved the yaw rate, and the vehicle side-slip angle has stayed in stability limits as well. Moreover, both the TVDs like ESC improve the stability, however STC-TVD shows the best handling performance while the 4WD-TVD is the worst like before.

In spite of satisfactory functioning of TVDs, there are several limitations in their applications. Unlike ESC, the TVDs try to stabilize cornering using driving and positive torque on wheels. Stabilization using positive torque sometime has unexpected results. To investigate some of these situations, two severe manoeuvres are illustrated. In the first manoeuvre, the vehicle is facing an obstacle and trying to avoid it, whereas there is another obstacle beside the vehicle's path. The vehicle is moving with speed $v_0 = 140\frac{km}{h}$ and the steering angle suddenly reached to the maximum value $\delta_f = 10°$. In the second manoeuvre, the vehicle is facing an obstacle but there is a transition from normal to slippery road condition when it is avoiding the obstacle. The vehicle speed is $v_0 = 80\frac{km}{h}$ and the steering angle suddenly reaches to $\delta_f = 6°$.

To compare the performance of different systems, five vehicle models are prepared. The passive model consists of a simple Transmission model in the absence of any TVD or ESC, three models equipped with three types of TVD strategies and one model has ESC. From Figure 21, it is seen that the best performance belongs to ESC. Unfortunately, all the three TVD strategies failed to control the stability of the vehicle. The main reason of priority of ESC in stabilizing the motion is that ESC not only controls the cornering dynamics based on the generation of yawing moment but with reducing the speed and lateral acceleration simultaneously. These two cases showed that in critical situations, ESC can control the vehicle; however, none of the TVDs is successful in stabilizing the cornering dynamic.

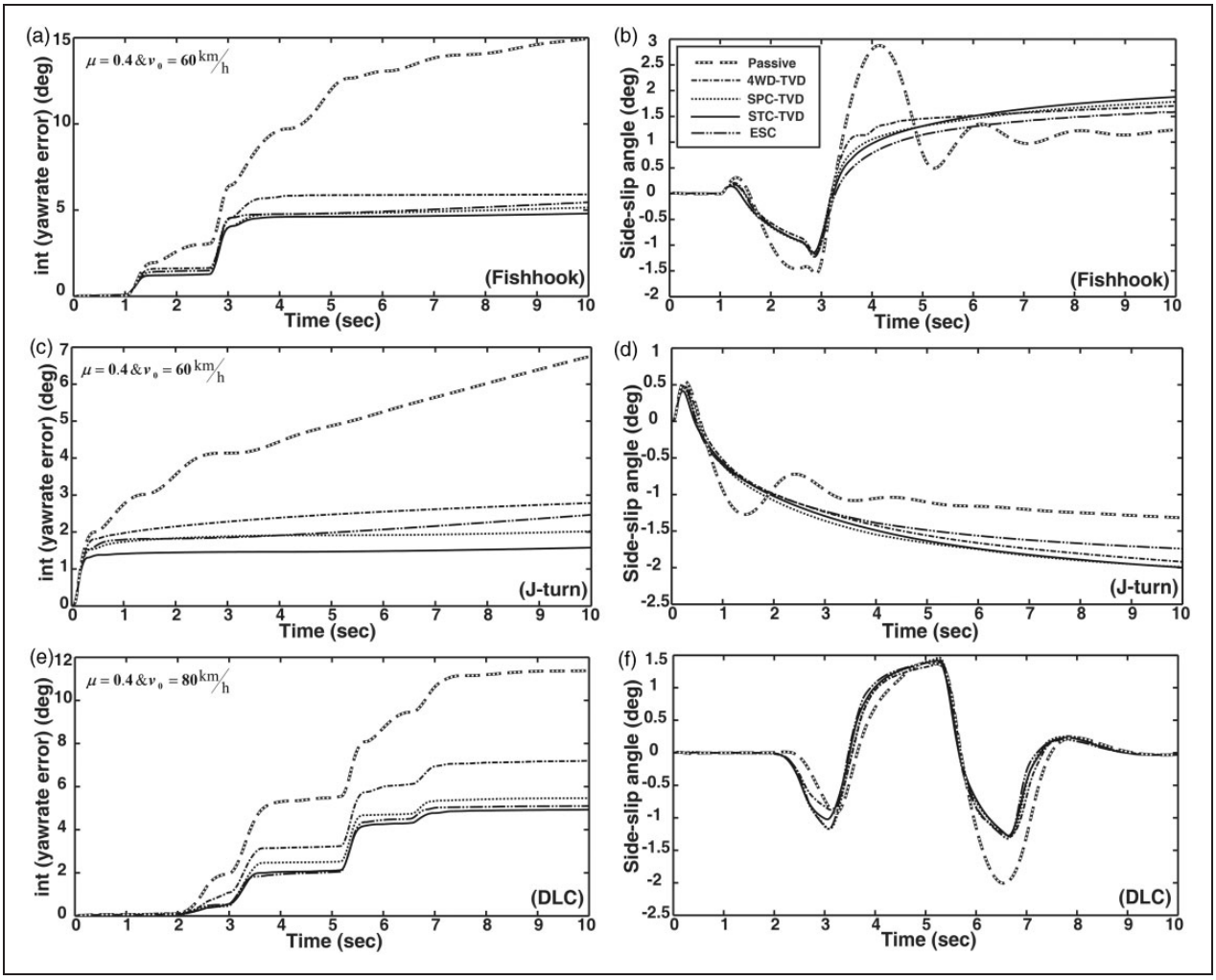

Figure 20. $\int_0^{10} |r - r_d| dt$ and side-slip angle for vehicle equipped with the torque distribution systems under wet road conditions.

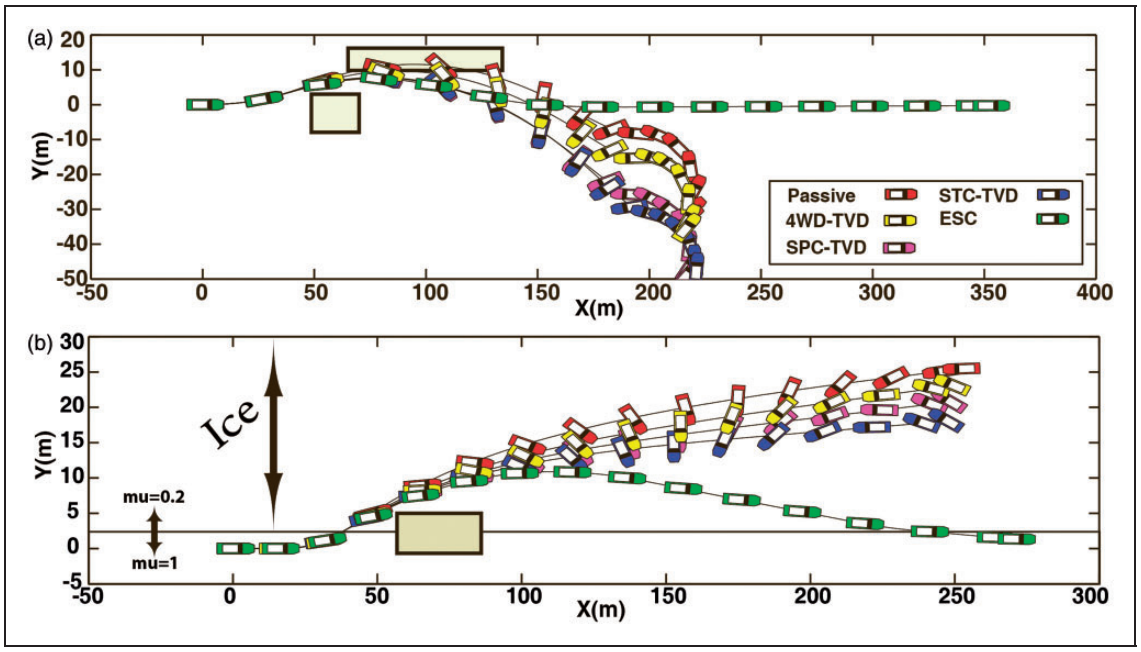

Figure 21. Performance of torque control systems in critical situations.

Conclusion

In this paper, different TVD strategies were introduced and their performance is compared under the control of an optimized fuzzy controller. The vehicle performances included handling, stability, fuel consumption, and ride comfort. The vehicle model consists of engine dynamics model, Pacejka tyre–road model, and transmission model, and an eight DOF mixed longitudinal and lateral dynamic model. Then three types of TVD strategies as well as ESC system were used as cornering and stability control system. Each system equipped with an optimized fuzzy control which is optimized using Bee's Algorithm. The main contributions of this research are summarized as below:

- Unless in the critical situations (high speed, high slip angle and low friction) in which the ESC has dominant stability control performance, in other situations TVD strategies show much better performance.
- STC-TVD shows the better handling performance.
- 4WD-TVD has better ride comfort as well as fuel consumption performance.
- SPC-TVD requires stronger actuator and larger set of clutches to generate the controlling torques.
- 4WD-TVD required the driving torque apply to the rear wheels to correct operation while there is no such limitation for SPC-TVD and STC-TVD.

Declaration of Conflicting Interests

The author(s) declared no potential conflicts of interest with respect to the research, authorship, and/or publication of this article.

Funding

The author(s) received no financial support for the research, authorship, and/or publication of this article.

References

1. Shibahata Y, Shimada K and Tomari T. Improvement of vehicle maneuverability by direct yaw moment control. *Vehicle Syst Dynam* 1993; 22: 465–481.
2. Piyabongkarn D, Lew JY, Rajamani R, et al. Active driveline torque-management systems. *Ctrl Syst Magazine, IEEE* 2010; 30: 86–102.
3. Hancock M. *Vehicle handling control using active differentials*. PhD thesis, University of Loughborough, UK, 2006.
4. Goodarzi A and Alirezaie M. Integrated fuzzy/optimal vehicle dynamic control. *Int J Automot Technol* 2009; 10: 567–575.
5. Papelis Y, Brown T, Watson G, et al. *Study of ESC assisted driver performance using a driving simulator*. University of Iowa, National Advanced Driving Simulator. 2004; 4: Document ID: N04-003-PR.
6. Goodarzi A, Rahiminejad D and Esmailzadeh E. Design of a fuzzy controller for independent control of front wheels steering angles. In: *ASME conference proceedings*, San Diego, California, 30 August–2 September 2009, pp.1061–1067.
7. Osborn RP and Shim T. Independent control of all-wheel-drive torque distribution. *Vehicle Syst Dynam* 2006; 44: 529–546.
8. Sawase K and Sano Y. Application of active yaw control to vehicle dynamics by utilizing driving/breaking force. *JSAE Rev* 1999; 20: 289–295.
9. Atsumi Y. Development of SH-AWD (super handling-all wheel drive) system. Honda/Tochigi R&D Center. Available at: https://www.hondarandd.jp/point.php?pid=249&lang=en (2005, accessed 15 July 2012).
10. Mimura K. *Differential gear*. USA, 2000.
11. Motoyama S, Uki H, Isoda K, et al. Effect of traction force distribution control on vehicle dynamics. *Vehicle Syst Dynam* 1993; 22: 455–464.
12. Ikushima Y and Sawase K. A study on the effects of the active yaw moment control. Detroit, Michigan: SAE International, 27 February–2 March 1995: Paper Number: 950303.
13. Hancock M, Williams R, Gordon T, et al. A comparison of braking and differential control of road vehicle yaw-sideslip dynamics. *Proc IMechE, Part D: J Automobile Engineering* 2005; 219: 309–327.
14. Deur J, Ivanović V, Hancock M, et al. Modeling and analysis of active differential dynamics. *J Dynam Syst Measure Ctrl* 2010; 132: 061501–061514.
15. Pacejka HB. *Tire and vehicle dynamics*. London: Butterworth-Heinemann, Elsevier, 2006, pp.186–190.
16. Mavros G, Rahnejat H and King P. Transient analysis of tyre friction generation using a brush model with interconnected viscoelastic bristles. *Proc IMechE, Part K: J Multi-body Dynamics* 2005; 219: 275–283.
17. Mavros G, Rahnejat H and King P. Analysis of the transient handling properties of a tyre, based on the coupling of a flexible carcass—belt model with a separate tread incorporating transient viscoelastic frictional properties. *Vehicle Syst Dynam* 2005; 43: 199–208.
18. Hegazy S, Rahnejat H and Hussain K. Multi-body dynamics in full-vehicle handling analysis. *Proc IMechE, Part K: J Multi-body Dynamics* 1999; 213: 19–31.
19. Centea D, Rahnejat H and Menday M. The influence of the interface coefficient of friction upon the propensity to judder in automotive clutches. *Proc IMechE, Part D: J Automobile Engineering* 1999; 213: 245–258.
20. Mechanical Simulation Corporation. Available at: www.carsim.com.
21. Jafri FA. *Nonlinear dynamics of controlled slipping clutches*. Cincinnati, PhD thesis, University of Cincinnati, USA, 2007.
22. Deur J, Petric J, Asgari J, et al. Modeling of wet clutch engagement including a thorough experimental validation. *SAE Transact* 2005; 114: 1013–1028.
23. Karnopp D. Computer simulation of stick-slip friction in mechanical dynamic systems. *J Dynam Syst Measure Ctrl* 1985; 107: 100–103.
24. Jaafari SMM. *Optimal control of torque splitter system for a 4WD vehicle for better handling*. MSc Thesis, Shahid Chamran University of Ahvaz, Iran, 2012.
25. VAN ZANTEN A. Bosch ESP systems: 5 years of experience. *SAE Transact* 2000; 109: 428–436.
26. Rajamani R. *Vehicle dynamics and control*. New York, NY: Springer, 2005, pp.221–256.
27. Wong JY. *Theory of ground vehicles*. New York: John Willey & Sons, 2001.

28. Shousong H. *Automatic control theory*. Beijing: Science Press, 2001.
29. Aoki Y, Uchida T and Hori Y. Experimental demonstration of body slip angle control based on a novel linear observer for electric vehicle. In: *31st annual conference of IEEE Industrial Electronics Society*, 2005, IEEE, Sheraton Capital Center Raleigh, NC, USA, 6–10 November 2005, p.6.
30. Åström KJ and Wittenmark B. *Adaptive control*. Mineola, New York: Courier Dover Publications, 2008.
31. Pham D, Ghanbarzadeh A, Koc E, et al. The bees algorithm–a novel tool for complex optimisation problems. *Intell Product Machine Syst* 2006; 2: 454–461.

Appendix I

Notations

${}^{u}\vec{a}_{G_s}, {}^{u}\vec{a}_{G_u}$	acceleration of the sprung and unsprung mass (m.s^{-2})
a, b	longitudinal distance from the front and rear axle to the centre of mass (m)
$C_{\alpha f}, C_{\alpha r}$	front/rear cornering stiffness (N.rad^{-1})
d_r, d_f	front/rear roll damping (N .m.rad^{-1}.s^{-1})
F_{Li}, F_{Ci}, N_i	longitudinal, lateral and vertical tyre forces labelled $i = RF, LF, RR, LR$(N)
g_i	gear ratio of the speed increasing device
h_r	height of the unsprung mass from the road surface (m)
h_s	height of the sprung mass above roll axis (m)
h_u	height of roll axis above the unsprung mass (m)
${}^{u}\vec{H}_{G_u}, {}^{s}\vec{H}_{G_s}$	angular momentum of unsprung and sprung mass
i	speed ratio of differential bevel gear
i_f, i_r	speed ratio of front and rear differential bevel gear, respectively
I_c	the moment of inertia of the ordinary differential (kg.m^2)
I_{car1}, I_{car2}	the moment of inertia of the left and right planetary carriers, respectively (kg.m^2)
I_{C1}	the moment of inertia of the left clutch (kg.m^2)
I_{C1}	the moment of inertia of the left clutch and the gear 3 (kg.m^2)
I_{C2}	the moment of inertia of the right clutch (kg.m^2)
I_{C2}	the moment of inertia of the right clutch and the gear 2 (kg.m^2)
I_{cf}	the moment of inertia of the front ordinary differential (kg.m^2)
I_{dg}	the moment of inertia of the gears 4,5 and 6 (kg.m^2)
I_{gc}	the moment of inertia of the gear 1 (kg.m^2)
I_i	the moment of inertia of the rear propeller shaft (kg.m^2)
I_{ir}	the moment of inertia of the rear bevel gear (kg.m^2)
I_{r1}, I_{r2}	the moment of inertia of the left and right ring gears, respectively (kg.m^2)
I_1, I_2	the moment of inertia of the rear left and rear right half shafts, respectively (kg.m^2)
$I^s_x, I^s_y, I^s_z, I^s_{xy}, I^s_{yz}$	sprung mass moment of inertia and product inertia (kg.m^2)
I_{s1}	the moment of inertia of left clutch and the left sun gear (kg.m^2)
I_{s2}	the moment of inertia of right clutch and the right sun gear (kg.m^2)
$I_{s2} = I_{s1}$	the moment of inertia of the gear 1 (kg.m^2)
$I_{r2} = I_{r1}$	the moment of inertia of the gear 4 (kg.m^2)
I^u_z	unsprung mass moment of inertia (kg.m^2)
I_w	wheel inertia (kg.m^2)
I_1, I_2	the moment of inertia of the rear left and rear right half shafts, respectively (kg.m^2)
I_1, I_2, I_3, I_4	the moment of inertia of the rear left, rear right, front left and front right half shafts, respectively (kg.m^2)
k_r, k_f	front/rear roll stiffness (N .m.rad^{-1})
K_{Trans}	kinetic energy of transmission system (J)
K_u	understeering parameter
L	wheel base (m)
M	total vehicle mass (kg)
M_{Zi}	self-aligning moment of wheel labelled $i = RF, LF, RR, LR$ (N.m)
m_s, m_u	mass of the sprung mass, mass of the unsprung mass (kg)
n_c	number of active friction surfaces
r, r_d	vehicle yaw rate and desired yaw rate (rad.s^{-1})
R_w, r_c	effective radius of wheel and effective radius of clutch (m)
t	wheel tread (m)
T_{Bi}	braking torque applied to wheel $i = RF, LF, RR, LR$ (N.m)
T_e, T_{er}	engine torque and torque supplied to rear axle (N.m)
T_{f2}, T_{f1}	clutch frictional torque right and left (N.m)
T_{req}	hydraulic torque (N.m)

T_{ti}	torque supplied to the wheels labelled $i = 1, 2, 3, 4$ (N.m)
u, s	the coordinate fixed to sprung and unsprung mass
U_{wi}, V_{wi}	longitudinal and lateral wheel centre velocities $i = RF, LF, RR, LR$ (m.s^{-1})
v_i	wheel centre lateral velocity labelled $i = RF, LF, RR, LR$ (m.s^{-1})
v_x, v_y	longitudinal and lateral velocities of the unsprung mass centre (m.s^{-1})
v_{x0}, v_{y0}	longitudinal and lateral initial velocities of the unsprung mass centre (m.s^{-1})
x_r	longitudinal distance from centre of sprung and unsprung mass (m)
Z_i $(i = 1 \ldots 4)$	THE number of teeth of the gears 1–4 in Figure 4
Z_i $(i = 1 \ldots 6)$	the number of teeth of the gears 1–6 in Figure 3
Z_r, Z_s	the number of teeth of the ring gear and sun gear, respectively
α_i	sideslip angle of the wheel labelled $i = RF, LF, RR, LR$
β_{thr}	different percentage of throttle position
δ_f	steering angle of front wheels (rad)
φ, θ	roll/yaw angle (rad)
κ	longitudinal slip of wheel
μ	road friction coefficient
ω_i	angular velocity of the wheel labelled $i = RF, LF, RR, LR$ (rad.s^{-1})
ω_e	motor speed (rad.s^{-1})
ω_{f2}, ω_{f1}	right/left clutch slip speed (rad.s^{-1})
ω_1, ω_2	angular velocity of the rear left and rear right wheels, respectively (rad.s^{-1})
$\omega_1, \omega_2, \omega_3, \omega_4$	angular velocity of the rear left, rear right, front left and front right wheels, respectively (rad.s^{-1})

Appendix 2

The ${}^u\vec{a}_{G_u}(i)$, ${}^u\vec{a}_{G_u}(j)$, ${}^u\vec{a}_{G_s}(i)$, ${}^u\vec{a}_{G_s}(j)$, ${}^s\dot{\vec{H}}_{G_s}(i)$, ${}^s\dot{\vec{H}}_{G_s}(j)$ and ${}^s\vec{H}_{G_s}(k)$ components are given as follows

$$\begin{aligned} {}^s\dot{\vec{H}}_{G_s}(i) = {} & I_x^s\ddot{\varphi} + I_{xy}^s \sin(\varphi)\ddot{\theta} + I_{yz}^s\dot{\theta}^2 - 2I_{yz}^s(\cos(\varphi))^2\dot{\theta}^2 \\ & + I_z^s\cos(\varphi)\sin(\varphi)\dot{\theta}^2 - I_y^s\cos(\varphi)\sin(\varphi)\dot{\theta}^2 \end{aligned} \tag{48}$$

$$\begin{aligned} {}^s\dot{\vec{H}}_{G_s}(j) = {} & I_{xy}^s\ddot{\varphi} + I_y^s\sin(\varphi)\ddot{\theta} + I_{yz}^s\cos(\varphi)\ddot{\theta} \\ & + I_y^s\cos(\varphi)\dot{\theta}\dot{\varphi} - 2I_{yz}^s\sin(\varphi)\dot{\theta}\dot{\varphi} \\ & + I_x^s\cos(\varphi)\dot{\theta}\dot{\varphi} + I_{xy}^s\cos(\varphi)\sin(\varphi)\dot{\theta}^2 \\ & - I_z^s\cos(\varphi)\dot{\theta}\dot{\varphi} \end{aligned} \tag{49}$$

$$\begin{aligned} {}^s\dot{\vec{H}}_{G_s}(k) = {} & I_{yz}^s\sin(\varphi)\ddot{\theta} + I_z^s\cos(\varphi)\ddot{\theta} + 2I_{yz}^s\cos(\varphi)\dot{\theta}\dot{\varphi} \\ & - I_z^s\sin(\varphi)\dot{\theta}\dot{\varphi} + I_{xy}^s\dot{\varphi}^2 + I_y^s\sin(\varphi)\dot{\theta}\dot{\varphi} \\ & - I_x^s\sin(\varphi)\dot{\theta}\dot{\varphi} - I_{xy}^s\dot{\theta}^2 + I_{xy}^s(\cos(\varphi))^2\dot{\theta}^2 \end{aligned} \tag{50}$$

$$\begin{aligned} {}^u\vec{a}_{G_s}(i) &= \dot{v}_x - \dot{\theta}v_y - \dot{\theta}^2x_r + \ddot{\theta}\sin(\varphi)h_s + 2\cos(\varphi)\dot{\theta}\dot{\varphi}h_s \\ {}^u\vec{a}_{G_s}(j) &= \dot{v}_y + \dot{\theta}v_x + \ddot{\theta}x_r + \sin(\varphi)\dot{\varphi}^2h_s \\ & \quad - \cos(\varphi)\ddot{\varphi}h_s + \dot{\theta}^2\sin(\varphi)h_s \\ {}^u\vec{a}_{G_s}(k) &= -\cos(\varphi)\dot{\varphi}^2h_s - \sin(\varphi)\ddot{\varphi}h_s \end{aligned} \tag{51}$$

$${}^u\vec{a}_{G_u}(i) = \dot{v}_x - \dot{\theta}v_y, \; {}^u\vec{a}_{G_u}(j) = \dot{v}_y + \dot{\theta}v_x \tag{52}$$

The vertical loads on the wheels can be expressed as equation (53)

$$\begin{aligned} & N_{LF} = N_{SF} - \Delta N_x - \Delta N_y, N_{LR} = N_{SR} + \Delta N_x - \Delta N_y, \\ & N_{RF} = N_{SF} - \Delta N_x + \Delta N_y, N_{RR} = N_{SR} + \Delta N_x + \Delta N_y \end{aligned} \tag{53}$$

The parameters used in the above equations are given as

$$N_{SF} = \frac{((m_u + m_s)g - m_s{}^u\vec{a}_{G_s}(k))c}{2L} \tag{54}$$

$$N_{SR} = \frac{((m_u + m_s)g - m_s{}^u\vec{a}_{G_s}(k))b}{2L} \tag{55}$$

$$\Delta N_x = \frac{H_T(j) + (m_u{}^u\vec{a}_{G_u}(i) + m_s{}^u\vec{a}_{G_s}(i))(h_u + h_r)}{2L} \tag{56}$$

$$\begin{aligned} H_T(j) = {} & (h_s m_s{}^u\vec{a}_{G_s}(i) + {}^s\dot{\vec{H}}_{G_s}(j))\cos(\varphi) \\ & - h_u m_u{}^u\vec{a}_{G_u}(i) - \sin(\varphi){}^s\dot{\vec{H}}_{G_s}(k) \end{aligned}$$

$$\begin{aligned} \Delta N_y = {} & \frac{H_T(i) - \sin\varphi(t)h_s m_s g}{2t} \\ & - \frac{(m_u{}^u\vec{a}_{G_u}(j) + m_s{}^u\vec{a}_{G_s}(j))(h_u + h_r)}{2t} \end{aligned}$$

$$\begin{aligned} H_T(i) = {} & h_u m_u{}^u\vec{a}_{G_u}(j) + {}^s\dot{\vec{H}}_{G_s}(i) - \sin(\varphi)h_s m_s{}^u\vec{a}_{G_s}(k) \\ & - \cos(\varphi)h_s m_s{}^u\vec{a}_{G_s}(j). \end{aligned} \tag{57}$$

According to Figure 1, the velocity at the centre of vehicle wheels is calculated from equation (58)

$$\begin{aligned} \vec{\boldsymbol{v}}_{\boldsymbol{LF}} &= \begin{bmatrix} v_x - \dot{\theta}t/2 \\ v_y + \dot{\theta}a \\ \dot{\theta} \end{bmatrix}, \quad \vec{\boldsymbol{v}}_{\boldsymbol{RF}} = \begin{bmatrix} v_x + \dot{\theta}t/2 \\ v_y + \dot{\theta}a \\ \dot{\theta} \end{bmatrix}, \\ \vec{\boldsymbol{v}}_{\boldsymbol{RR}} &= \begin{bmatrix} v_x + \dot{\theta}t/2 \\ v_y - \dot{\theta}b \\ \dot{\theta} \end{bmatrix}, \quad \vec{\boldsymbol{v}}_{\boldsymbol{LR}} = \begin{bmatrix} v_x - \dot{\theta}t/2 \\ v_y - \dot{\theta}b \\ \dot{\theta} \end{bmatrix}. \end{aligned} \tag{58}$$

So the slip angle of the wheels is calculated from equation (59)

$$\alpha_{LF} = \tan^{-1}\left(\frac{v_y + \dot{\theta}a}{v_x - \dot{\theta}t/2}\right) - \delta_f, \alpha_{LR} = \tan^{-1}\left(\frac{v_y - \dot{\theta}b}{v_x - \dot{\theta}t/2}\right),$$
$$\alpha_{RF} = \tan^{-1}\left(\frac{v_y + \dot{\theta}a}{v_x + \dot{\theta}t/2}\right) - \delta_f,$$
$$\alpha_{RR} = \tan^{-1}\left(\frac{v_y - \dot{\theta}b}{v_x + \dot{\theta}t/2}\right). \quad (59)$$

The wheel equation of motion is calculated from equation (60)

$$I_w\omega_i = T_i - R_wF_{Li}, \quad i = LF, LR, RF, RR. \quad (60)$$

In equation (60), T_i is the torque transfer to the wheel, R_{wi} is effective radius of wheel and I_{wi} is moment of inertia of wheel.

The longitudinal slip is calculated from equation (61)

$$\kappa_i = \frac{|R_{wi}\omega_i - U_{wi}|}{U_{wi}}. \quad (61)$$

In equation (61), ω_i is angular velocity and U_{wi} is the velocity of each wheel hub in the rolling direction of that wheel that can be derived from equation (62)

$$\mathrm{U_{WRF}} = (v_x + \dot{\theta} \times \frac{t}{2})\cos(\delta) + (v_y + \dot{\theta} \times b)\sin(\delta_f),$$
$$\mathrm{U_{WLR}} = \left(v_x - \dot{\theta} \times \frac{t}{2}\right)$$
$$\mathrm{U_{WLF}} = \left(v_x - \dot{\theta} \times \frac{t}{2}\right)\cos(\delta) + (v_y + \dot{\theta} \times b)\sin(\delta_f),$$
$$\mathrm{U_{WRR}} = \left(v_x + \dot{\theta} \times \frac{t}{2}\right) \quad (62)$$

Stribeck equation

μ_F (in equation (7)) is described by the Stribeck equation that is given in equation (63).[3]

$$\mu_F = [\mu_c + (\mu_s - \mu_c)e^{-[|\omega_f|/\omega_s]^k} + \beta_v|\omega_f|]\mathrm{sgn}(\omega_F) \quad (63)$$

In equation (63), μ_c, μ_s and β_v are the Coulomb friction, static friction and viscous friction coefficients, respectively. ω_f is the relative speed between clutch plates and ω_s and k are the Stribeck coefficients. The parameters used in equation (63) are given in Table 2.

Table 2. Stribeck coefficients parameters.[3]

k	ω_s	β_v	μ_s	μ_c
1	2	0.0032	1.2	0.9

Table 3. Numerical values of the vehicle parameters.

$t = 1.55$ (m)	$b = 1.63$ (m)	$a = 1.13$ (m)
$h_r = 0.3$ (m)	$h_u = 0.1$ (m)	$h_s = 0.14$ (m)
$I_x^s = 606$ (kgm^2)	$m_s = 160$ (kg)	$m_s = 1369$ (kg)
$I_x^u = 100$ (kgm^2)	$I_z^s = 3791$ (kgm^2)	$I_y^s = 4191$ (kgm^2)
$R_w = 0.3$ (m)	$I_z^u = 450$ (kgm^2)	$I_y^u = 200$ (kgm^2)
$d_f = 2000$ (Nms rad)	$k_r = 30,000$ (Nms rad)	$k_f = 30,000$ (Nms rad)
$g = 9.81$ (m/s^2)	$I_w = 0.9$ (kgm^2)	$d_f = 2000$ (Nms rad)

Table 4. Numerical values of the SPC-TVD mechanism parameters.[14]

$h_2 = 1.125$	$h_1 = 0.875$	$I_i^* = 0.15$ (kgm^2)
$I_2 = 0.05$ (kgm^2)	$I_1 = 0.05$ (kgm^2)	$i = 2.8$

Table 5. Numerical values of the STC-TVD mechanism parameters.[14]

$h_2 = 1.125$	$h_1 = 1.125$	$I_i^* = 0.15$ (kgm^2)
$H_{12} = 3.5$	$H_{11} = 4.5$	$I_i^* = 0.15$ (kgm^2)
$I_{c1} = 0.002$ (kgm^2)	$H_{22} = 3.5$	$H_{21} = 4.5$
$I_{r2} = 0.001$ (kgm^2)	$I_{r1} = 0.001$ (kgm^2)	$I_{c2} = 0.002$ (kgm^2)
$I_2 = 0.05$ (kgm^2)	$I_1 = 0.05$ (kgm^2)	$i = 2.8$

Table 6. Numerical values of the 4WD-TVD mechanism parameters.[14]

$h_2 = 2.6$	$h_1 = 2.6$	$J = 0.25$ (kgm^2)
$I_{s2} = 0.002$ (kgm^2)	$I_{s1} = 0.002$ (kgm^2)	$g = 1.05$
$I_4 = 0.05$ (kgm^2)	$I_3 = 0.05$ (kgm^2)	$i_f = 2.8$

Table 7. Linguistic terms of fuzzy controller.

Positive low	ZP	Negative low	ZN	Zero	Z
Negative very high	N3	Negative high	N2	Negative medium	N1
Positive very high	P3	Positive high	P2	Positive medium	P1

Appendix 3

The numerical values of vehicle model and the active differentials parameters are given in Tables 3–6.

Table 8. Performance of the control system.

Error	δ_f	Fuzzy output	Vehicle status	TVD Clutching	ESC Braking
$e < 0$	$\delta_f > 0$	Positive	Understeer	Right clutch	Rear-left
$e < 0$	$\delta_f < 0$	Positive	Oversteer	Right clutch	Front-left
$e > 0$	$\delta_f > 0$	Negative	Oversteer	Left clutch	Front-right
$e > 0$	$\delta_f < 0$	Negative	Understeer	Left clutch	Rear-right

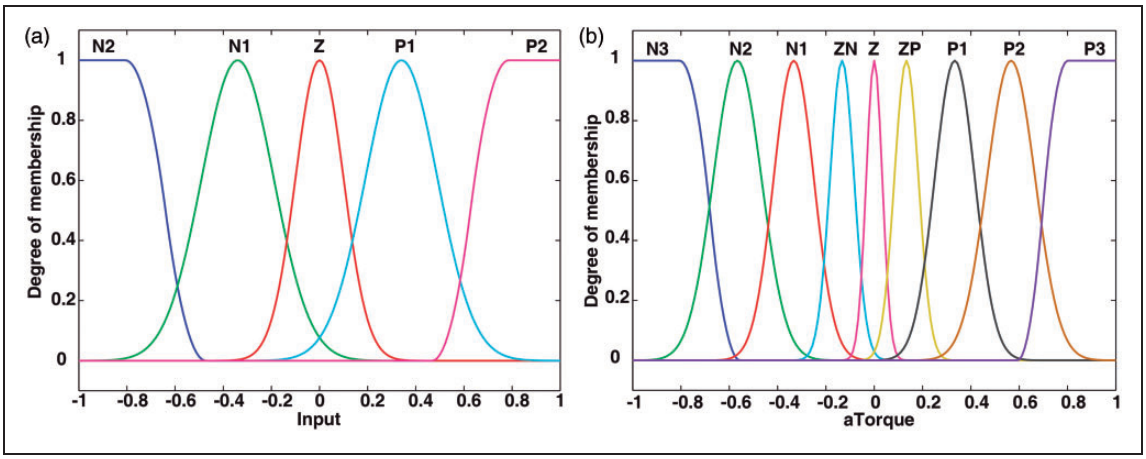

Figure 22. (a) Input membership functions and (b) output membership functions for the fuzzy controller.

Table 9. Fuzzy rule base.

			e				
β		$\dot{e}$	N2	N1	Z	P1	P2
Low	Z	N2	P3	P2	P1	ZP	Z
		N1	P2	P1	ZP	Z	ZN
		Z	P1	ZP	Z	ZN	N1
		P1	ZP	Z	ZN	N1	N2
		P2	Z	ZN	N1	N2	N3
Medium	P1	N2	P3	P2	P1	P1	ZP
		N1	P2	P1	ZP	ZP	Z
		Z	P1	ZP	Z	Z	ZN
		P1	ZP	Z	ZN	ZN	N1
		P2	Z	ZN	ZN	N1	N1
	N1	N2	P1	P1	ZP	ZP	Z
		N1	P1	ZP	ZP	Z	ZN
		Z	ZP	Z	Z	ZN	N1
		P1	Z	ZN	ZN	N1	N2
		P2	ZN	N1	N1	N2	N3
High	P2	P3	P3	P3	P3	P3	
	N2	N3	N3	N3	N3	N3	

Appendix 4

To set the fuzzy controller a Gaussian membership function, Mamdani inference engine and centre of gravity defuzzification method have been employed. The abbreviations used in fuzzy rules and membership functions are given in Table 7. Table 8 shows the performance of the controller in selecting the appropriate clutching or braking. Positive fuzzy output means that positive yaw moment is generated, and the negative one means that the yaw moment is negative. Input and output normalized membership functions (of non-optimized controller) are shown in Figure 22(a) and (b). Fuzzy rules (of non-optimized controller) used to control the torque control systems are given in Table 9.